



Durham E-Theses

Nano Structure and Novel Charging Materials of the Small Molecule Based OLED Devices

CHIANG, CHIEN-JUNG

How to cite:

CHIANG, CHIEN-JUNG (2007) *Nano Structure and Novel Charging Materials of the Small Molecule Based OLED Devices*, Durham theses, Durham University. Available at Durham E-Theses Online: <http://etheses.dur.ac.uk/160/>

Use policy

The full-text may be used and/or reproduced, and given to third parties in any format or medium, without prior permission or charge, for personal research or study, educational, or not-for-profit purposes provided that:

- a full bibliographic reference is made to the original source
- a [link](#) is made to the metadata record in Durham E-Theses
- the full-text is not changed in any way

The full-text must not be sold in any format or medium without the formal permission of the copyright holders.

Please consult the [full Durham E-Theses policy](#) for further details.

**Nano Structure and Novel Charging Materials of the
Small Molecule Based OLED Devices**

Chien-Jung Chiang

A thesis submitted to the Faculty of Science, The University of Durham, for
the degree of Master of Science

Organic Electroactive Materials Group
Department of Physics
University of Durham
May 2007

Declaration

All material contained in this thesis is original and is the result of my own work except where explicit reference is made. Material from work of others has been suitably indicated.

This thesis has not been submitted in whole or in part for the award of a degree at this or any other university.

The copyright of this thesis rests with the author. No quotation from it should be published without their prior consent and information derived from it acknowledged.

Acknowledgements

I want to thank all the people who have supported me during my MSc course and who have made this work possible.

I want to thank my supervisor, Professor Andy P. Monkman, who gives me the opportunity to study and live in this beautiful city of Durham, and always supplies all I need for my research.

I want to thank my parents for their full support of my study financially and spiritually.

I want to thank my wife, Mun-Ying, for her accompanies to allow me to focus on my research fully.

I want to thank, last but not least, Dr. Carsten Rothe, for his guidance in research, and as friend, to spend a lot of great time together after work.

Abstract

This work introduces the process of fabricating a conventional bilayer-structured small molecule based Organic Light Emitting Diode (OLED) device by vacuum thermal deposition technology using a Kurt J. Lesker deposition machine. The system was calibrated carefully by determining the tooling factor of all the materials that were used. The indium-tin-oxide (ITO) coated glass substrates with a thin layer of polycarbonate (PC) template overlaid were supplied by Dr. Etienne Ferain of Université catholique de Louvain, Belgium. In the PC film, an array of consistently structured, randomly distributed nanopores with diameter up to 110 nm were produced and used as a mask to fabricate the nano-OLEDs. The device was then tested and compared to a normal scaled OLED device. To further prove the fabrication of nano-OLEDs, images of Scanning Electron Microscope (SEM) and Atomic Force Microscope (AFM) measurements were presented.

Finally, a set of iridium complexes synthesized by Professor Martin Bryce's group in the Chemistry Department of Durham University were spin-coated onto the ITO/Glass substrate to make an OLED device. Such complexes, while in devices, behave as the electrolyte. When a Voltage bias was applied to a system with a heavy cation and light anion, the light anions will flow toward the anode to form a built-in voltage across the system. The charge carriers injecting barrier is thus lowered to enhance the electroluminescence (EL) performance of the OLED device. Devices made from 5 different iridium complexes were produced and measured in the course of this work. The highest efficiency achieved was 7.8 cd/A @ 9V with a simple aluminum / iridium complex / Poly(3,4-ethylenedioxythiophene) poly(styrenesulfonate) (PEDOT:PSS) / ITO structure.

Table of Contents

Acknowledgement.....	3
Abstract.....	4
Chapter 1 Introduction.....	7
Chapter 2 Experimental.....	16
2.1 Thermal Evaporation: Thin-Film Deposition Methods.....	16
2.2 Spin-Coating Deposition	18
2.3 Substrate Preparation.....	19
2.4 Electrical and Optical Measurement.....	20
Chapter 3 Preliminary.....	22
3.1 Parameter Determination.....	22
3.1.1 Determination of the film thickness by QCM	22
3.1.2 Tooling factor	23
3.1.3 Z factor.....	24
3.1.4 Unknown materials.....	26
3.2 Film Thickness Detection by Interferometry.....	27
3.2.1 Theory.....	27
3.2.2 Detecting steps.....	28
3.3 The Fabrication of the Reference OLED Device.....	29
3.3.1 The fabrication.....	31
3.3.2 Results and summary.....	32
Chapter 4 Phosphorescent Organic Light-Emitting Nano Diodes.....	37
4.1 Introduction.....	37

	4.2 Fabrication and Experimental.....	38
	4.3 Results and Discussion.....	39
	4.4 Summary.....	47
Chapter 5	High Efficiency Charged Iridium Metal Complex Based Light-Emitting Diodes.....	49
	5.1 Introduction.....	49
	5.2 Experimental.....	53
	5.2.1 Sample preparation.....	53
	5.2.2 Analysis method.....	54
	5.3 Results and Discussion.....	55
	5.3.1 Comparison of different cathode material with complexes in family 1 as light emitting layer.....	55
	5.3.2 Comparison of different cathode material with complexes in family 2 as light emitting layer.....	63
	5.3.3 Summary.....	74
	5.3.4 Comparison of different ligands.....	76
	5.3.5 Phosphorescence lifetime studies	80
	5.3.6 Highlight of the LEC devices.....	82
	5.4 Conclusion.....	84

Chapter 1

Introduction

The 21st century is the century of communication when people carry along with them the information of the whole world every second, everywhere. We can say that we live in an age of 4C's: computer, communication, consumer electronics, and car electronics. With the help of 3G technologies, the need for a smaller, lighter, mobile display is obvious.

Recently organic light emitting diodes (OLEDs) technology has become one of the most powerful candidates in the competition of flat display applications. Advantages include self-emitting, wide viewing angle (over 170 degree), fast reaction time (less than 1 μ s), high efficiency, low operation voltage (3-10V), slim (down to 2mm thick), flexible in shape, and easy to produce. A comparison of OLED with other candidate technologies is listed in [table 1.1](#).



Fig. 1.1 Sony XEL-1 11" OLED TV. (image from <http://blogs.mirror.co.uk/techno-techno/2008/08/ifa-2008-sony-go-super-slim-wi.html>)

	Cathode Ray Tube (CRT)	Liquid Crystal Display (LCD)	OLED	Light Emitting Diode (LED)	Plasma Display Panel (PDP)
Brightness	G	G	VG	N	N
Efficiency	G	G	VG	N	N
Life	VG	G	G	VG	N
Weight	B	VG	VG	N	G
Thickness	B	VG	VG	N	G
Reacting Time	VG	N	VG	VG	G
View Angle	VG	B	VG	N	N
Cost	VG	G	G	G	N

Table 1.1 Evaluation of the main players in the new generation display competition.

VG: very good; G: good; N: normal; B: bad

Although the development of Liquid Crystal Display (LCD) technology has improved both the viewing angle and reaction time, the fact that OLEDs have a higher power efficiency and wider range of operating temperatures (between -40 to 85 °C) does give some advantages in specific tasks. Furthermore, for smaller display panels used on mobile phones, the small viewing angle problem for LCD still has no solution. Therefore OLED or Poly-LED (similar to OLED but with long chain polymer as the functional

layer) devices have a huge potential to take over the world's flat display and lighting market.



Fig. 1.2. Sony NWZ 1050 touch-screen OLED MP3 player. (image from <http://www.itechnews.net/tag/sony-nwz-x1050/>)

In 1963, Professor Pope reported the electroluminescence (EL) of anthracene crystals under more than 700 volts driving voltage¹. This was the first article related to organic EL. But because of the very high drive voltage and bad efficiency, no further investigation was made of this material until 1987. In 1987 Dr. Ching W. Tang and Dr. Steve Vanslyke of Kodak LTD. developed a multi-layer small molecule based OLED device using thermal deposition technology². This design attracted the world's attention with its low operating voltage (6 V) and high efficiency (1 cd/A) by successfully confining the excitons (the electron-hole pairs) at the interface of a Hole Transporting Layer (HTL) and an Electron Transporting Layer (ETL) to emit light.

In 1990, Professor Richard Friend and J. Burroughs of Cambridge University successfully fabricated Poly-LEDs based on conjugated polymers deposited by spin-coating method³. This very easy process can be operated in air instead of in a high vacuum, which is required for thermal deposition processes. This discovery again showed the world the huge potential of the self-emitting organic species, but also raised another big question: should we go for OLEDs or Poly-LEDs?

An OLED device usually consists of several functional layers and one or more major emitter layers, which are finally sandwiched by two electrodes as shown in the [Fig. 1.3](#). When a voltage bias is applied, the charge carriers are injected into the functional layers by overcoming the potential barrier between the electrode work function and the energy state of the highest occupied molecular orbital (HOMO) or the lowest unoccupied molecular orbital (LUMO). The injected electrons and holes are driven by the electric field, and hopping from one molecule to another. Some of them will be trapped by the empty energy state of defects, some will travel all the way to the other electrode and generate heat, the rest would meet each other and form the electron-hole pairs (excitons).

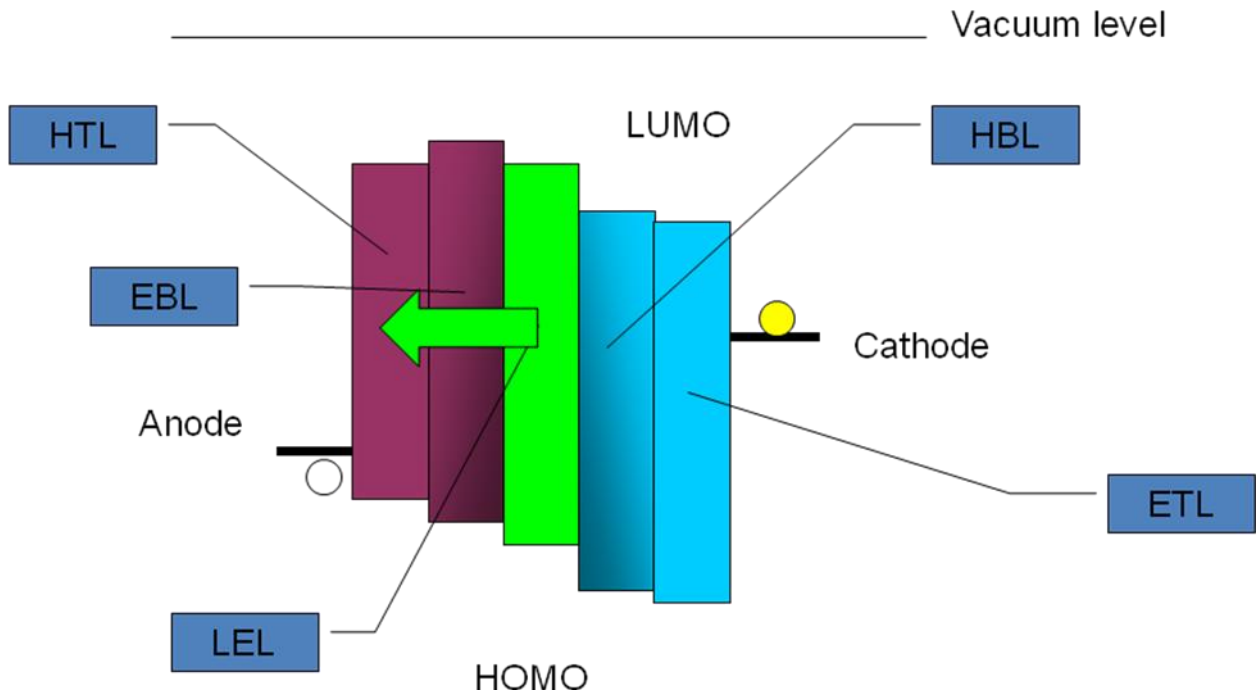


Fig. 1.3 The typical energy structure of an OLED device. The open circle is the free hole, and the yellow circle is the free electron. HTL: Hole Transporting Layer; EBL: Electron Blocking Layer; LEL: Light Emitting Layer; HBL: Hole Blocking Layer; ETL: Electron Transporting Layer.

Generally speaking, only 25% of these excitons will be in singlet state as required by quantum mechanics, and recombine to emit light. The other 75% of the excitons, which are in a triplet state, would have a longer lifetime (up to milliseconds) than their singlet counterparts because of the forbidden T_1 (triplet state) $\rightarrow S_0$ (ground state) transition. This allows them to migrate in the bulk for up to several nano-meters⁴. They may either transfer to lower energy states or recombine to pass energy to the surrounding lattice (heat) or collide with each other to form another singlet exciton (triplet-triplet

annihilation)⁵⁻⁶. Energy transferring routes for the excitons are shown in Fig. 1.4.

Therefore, the question of how to make the most of the injected electrons and holes to form excitons, and how to get most of the excitons to emit light at the wavelength one wants, has become the Holy Grail for OLED researchers.

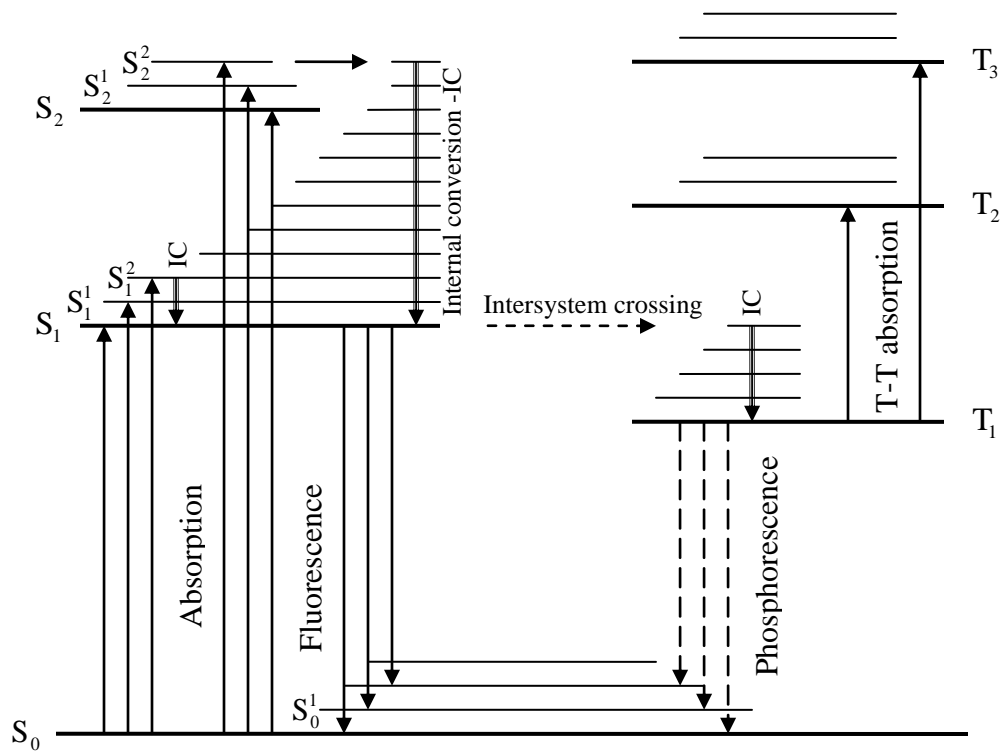


Fig. 1.4 The Jablonski diagram shows all the energy transferring routes of the exciton.

S denotes the singlet state, and T denotes the triplet state.

In the last decade, the performance of OLED devices has improved significantly in many creative ways. Some of the most important examples are highlighted as follows:

1. Better matching of the energy levels between each functional layer, especially between the electrode and its adjacent layer⁷.
2. The inclusion of the hole and electron blocking layers to achieve better charge carrier balance⁸.
3. Recycling the triplet excitons (75% of all excitons created) by doping an energy matching material into what we now called the “host” material to an optimized density and thus emit light through the dopant species⁹.
4. Design the optical structure by depositing high refractive index material outside of the transparent electrode to extract the most of the out coupled light¹⁰.

As a result, OLEDs are gradually approaching the stage of mass production: In 2006 organic EL panel shipments has reached \$530 million (USD). The year 2008 saw the release of an OLED TV, Sony's XEL-1, which is rated at a 30,000 hours lifetime - or 8 hours a day for 10 years. On the other hand, the Poly-LEDs, which are more preferable here in the UK, have gradually become reality in the last few years too. Poly-LEDs could only be fabricated with one layer because of the limitation of the spin-coating method: when one material is dissolved and spin-coated as the thin-film, it is difficult to spin-coat another material onto it without dissolving the already-laid material. Chemists, therefore, can only modify side-chains attached to the main bone of the conjugated polymer to achieve the better charge carrier balance or quantum yield. This, however, had been solved by a group in Taiwan lead by Professor Meng of National Chiao-Tung University.

They introduced a new process of fabrication and spin-coated more than one layers to successfully increase the efficiency of a deep blue emitter to 1.5 cd/A¹¹. Companies such as Epson have also developed a method of “Inkjet Printing” to replace the original spin-coating process. The new process allows large-area deposition through a special printer. All these efforts have secured the Poly-LEDs’ position as one of the front-runners in the competition of “greener” lighting source of the future.

The pros of OLEDs are their controllable process of fabrication. Everything is done in a vacuum and the deposition rate and final thickness of the layers are all monitored precisely. These pros can also become cons; the process is costly. The pros of Poly-LEDs, however, are that simple single-layer spin-coating (or inkjet-printing) does not need a vacuum and can be carried out in the air. It is cheaper but less reliable and repeatable¹². So it is clear that each type of device still has its own problems to be solved.

In this thesis, both OLED and Poly-LED are explored for different applications. In Chapter 2, the details of the device fabrication using thermal evaporation and spin coating are given. The calibration of the experiment is described in Chapter 3. In Chapter 4, OLEDs are fabricated in the nano-scale as the controllable deposition process makes it possible. Finally, in Chapter 5, charged iridium complexes were used to fabricate Poly-LED devices and different designs of structure were tested to produce comparable EL performance to conventional OLED devices.

References:

1. M. P. a. H. K. M. Sano, *Journal of Chemical Physics* **43** (8), 2920-2921 (1965).
2. C. W. T. a. S. A. Vanslyke, *Applied Physics Letters* **51** (12), 913-915 (1987).
3. D. D. C. B. J. H. Burroughes, A. R. Brown, R. N. Marks, K. Mackay, R. H. Friend, P. L. Burns, A. B. Holmes, *Nature* **347**, 539-541 (1990).
4. C. Rothe and A. P. Monkman, *Physical Review B* **68** (7) (2003).
5. S. M. King, D. Dai, C. Rothe and A. P. Monkman, *Physical Review B* **76** (8) (2007).
6. C. Rothe, S. King and A. P. Monkman, *Physical Review B* **73** (24) (2006).
7. F. C. Wang, S. Liu, H. L. Zhou, S. Sun, B. L. Qi and G. P. Ou, *Microelectron. J.* **37** (9), 916-918 (2006).
8. Z. Y. Xie, L. S. Hung and S. T. Lee, *Applied Physics Letters* **79** (7), 1048-1050 (2001).
9. C. Adachi, M. A. Baldo, S. R. Forrest and M. E. Thompson, *Applied Physics Letters* **77** (6), 904-906 (2000).
10. W. X. Li, R. A. Jones, S. C. Allen, J. C. Heikenfeld and A. J. Steckl, *Journal of Display Technology* **2** (2), 143-152 (2006).
11. S. R. Tseng, S. C. Lin, H. F. Meng, H. H. Liao, C. H. Yeh, H. C. Lai, S. F. Horng and C. S. Hsu, *Applied Physics Letters* **88** (16) (2006).
12. S. R. Forrest, *Nature* **428**, 911-918 (2004).

Chapter 2

Experimental

2.1 Thermal Evaporation: Thin-Film Deposition Methods

Film deposition, by thermal evaporation, was first reported in 1887 by Nahrwold, who successfully deposited platinum films by sublimation in a vacuum¹. In the past 50 years the number of vacuum deposition techniques has multiplied and thin film uses have grown exponentially. Many modern products for consumer, commerce, military, medical, or research applications depend on thin films. The methods used to deposit thin films are split into: Physical Vapour Deposition (PVD) and Chemical Vapour Deposition (CVD) depending on the underlying principles causing film deposition. A PVD method evaporates or sputters a material, producing a gaseous plume or beam that deposits a film on the substrate. A CVD method uses reactive, volatile compounds that decompose on a heated substrate. Starting materials are often organo- or hydrido-compounds that pyrolyse at relatively low temperatures into a non-volatile (film) component and a pumpable vapour/gas. Both methods sub-divide into a variety of techniques with auxiliary mechanisms to achieve specific goals. The method used in our lab is more like PVD, or so the called the thermal evaporation method. So here this method will be introduced in more detail.

Thermal evaporation is a major thin film deposition technique particularly in R&D applications where low installation costs and inexpensive, disposable evaporant

'containers' are clear advantages. The disadvantages are that precise temperature control may not be simple and refractory metals sometimes alloy, unexpectedly, with evaporants (evaporating Al from a W boat for example). It is necessary to define the word 'evaporation' first. Almost all information about thin film deposition characterizes material transfer from bulk-to-film as evaporation. However the correct usage of evaporation covers the 'change of state' from a liquid to gas. A 'change of state' from a solid to gas should be called sublimation. In general thin film work, however, the physical state of the bulk material is of little consequence and is probably unknown. Throughout the thesis the word 'evaporation' covers both phenomena. A common misconception is that an evaporant's vapour pressure somehow changes markedly during a transition from sublimation to evaporation. That is, a solid evaporant at its melting point has a different vapour pressure when compared to the liquid form at its melting point. This is simply not true, for any material the vapour pressure versus temperature curve is smooth at all temperatures. To give an example from everyday experience, in a glass containing ice cubes and water at 0°C, both phases have exactly the same vapour pressure. To deposit thin film in Durham University, a Kurt. J. Lesker. Spectros II deposition system was used. The main operation vacuum chamber featured 6 thermal heating sources for organic material and another 3 for the metal. It can be pumped down to about 1×10^{-7} mbar and allows two different organic materials to be evaporated at the same time. The control panel is using the Sigma Instruments controllers software. The change of the shadow-mask during operation without breaking the vacuum is also possible with this system.

2.2 Spin-coating Deposition

Spin-coating is a procedure used to apply uniform thin films to flat substrates. In short, an excess amount of a solution is placed on the substrate, which is then rotated at high speed in order to spread the fluid by centrifugal force. A machine used for spin coating is called a spin coater, or spinner. Rotation is continued while the fluid spins off the edges of the substrate, until the desired thickness of the film is achieved. The applied solvent is usually volatile, and simultaneously evaporates. Generally, the higher the angular speed of spinning or the smaller the concentration of the solution, the thinner the film. This method can be used to create thin films with thicknesses below 10 nm.

The plain substrate or ITO coated substrates were cleaned successively with acetone and isopropanol, and placed upon the spin-coating stage (as level as possible), on which the polymer-solvent solution was dropped using the syringe with a 0.45 μm filter attached to achieve the best film quality. The plate was then spun in at least two stages which could be programmed into the spin-coating facility. During the first stage, the plate was spun at a low to moderate speed 500-1000 rpm for 5-10 seconds to evenly spread the solution. The thickness of the coating was then determined and controlled during the second stage by spinning the coating at a higher speed, between 1500-3000 rpm for anywhere between a few seconds and a minute. These conditions produce high quality coatings of Polymer for about 100 nm thick applying calibrated concentration of the solution.

Once spin-coating is complete, the plate is placed onto a hot plate (heated to around 100 °C) for several seconds or minutes to remove the excess solvent from the solid coating. The device is then baked for several hours in a vacuum oven at a temperature high enough to sufficiently remove the remaining solvent (70 °C) to complete the whole procedure. Although the spin-coating procedure is best used in a clean-room environment (Class 10 or 100), for many simple laboratory experiments, spin-coating may be performed directly in a clean fume hood. When compared with the thermal evaporating method, it is an advantage of Poly-LED devices.

2.3 Substrate Preparation

The cleanness of the substrate is very crucial for both OLED and Poly-LED devices. The devices tend to degrade from the contaminated area and the degradation spreads to the whole device very quickly². The standard chemical washing procedure is as follows:

1. Put the ITO/Glass substrate in the beaker and put the beaker in the ultrasonic bath.
2. Fill the beaker with deionized water (to remove the detergent), detergent (to remove oil), acetone (to remove most of the chemical contaminant), and isopropanol in sequence for 5 minutes each.
3. Load the substrate into the UV-Ozone box for 5 min. This treatment is proved to further lower the work function of ITO to 5.1 eV³⁻⁴.

2.4 Electrical and Optical Measurement

Current-Voltage characteristic and Brightness measurements:

A Keithley2400 was used as the current source to drive the devices and a Keithley2000 digital multi-meter measures the signal from a photodiode which is located in front of the device emitting area to detect the electrical luminescence. A slot for a focus lens between the photodiode and the device was added to strengthen the signal when the EL luminescence is too weak (less than 75cd/m^2) as shown in Fig. 2.1. The length of the emitting area divided by the distance from it to the lens is about 1/15, so when a lens is used, the incidence light will be collected within the range of 4 degree, therefore the angular dependence can be neglected. The Minolta LS100 Luminescence Meter is attached to the black measurement case as shown in Fig. 2.2. It is used to calibrate the signal collected by the photodiode (V) to the brightness (cd/m^2).

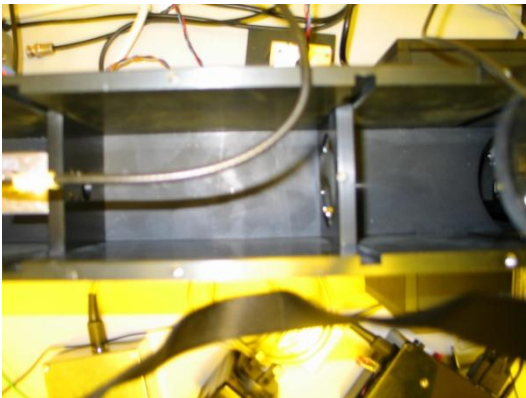


Fig. 2.1. The main measuring case viewed from above. The photodiode used to measure the luminescence signal is at the far left. The device holder is at the far right, and the focus lens used to strengthen the out coupling light is in the middle.



Fig. 2.2. The Minolta LS100 Luminescence Meter (right) is attached to calibrate the signal obtained by the photodiode to the brightness.

EL Spectrum measurement:

The EL spectra were obtained using the Ocean Optics USB 2000 device, which is connected to the back of the black measurement case through the optical fibre.

References:

1. R. Nahrwold, Ann. Physik **31**, 467 (1887).
2. H. Aziz and G. Xu, Synthetic Metals **80** (1), 7-10 (1996).
3. Y. Park, V. Choong, Y. Gao, B. R. Hsieh and C. W. Tang, Applied Physics Letters **68** (19), 2699-2701 (1996).
4. W. K. C. S.K. So, C.H. Cheng, L.M. Leung and C.F. Kwong, Applied Physics A **68**, 447-450 (1999).

Chapter 3

Preliminary Investigation

3.1 Parameter Determination

In order to evaporate the thin-film to the required thickness, there are 3 parameters that need be determined beforehand: tooling factor, film density, and Z-Factor (acoustic impedance). Except for the film density, which is explained by its name - the density of the thin-film, the other two parameters are to be introduced in this chapter. But before that, the technique of Quartz Crystal Microbalance (QCM) which is used to detect the thickness of the evaporated film in our evaporation system should be introduced first.

3.1.1 Determination of the film thickness by QCM

The thickness of the deposited film during the thermal evaporation is determined by the QCM. In an electronic oscillator circuit, a quartz crystal's natural resonant frequency determines the frequency of oscillation of the circuit. The quartz crystal is located in the vacuum deposition system and above the thermal evaporating source. The relative position between the substrate and the quartz sensor is shown in Fig. 3.1. As the material is deposited on both the substrate and the crystal, the crystal becomes thicker and the resonant frequency decreases.

Equation 3.1, the so called the QCM Equation, correlates this frequency change with film thickness. Deposition rate is then derived from thickness, by dividing the change in thickness by the time period between measurements.

$$T_f = \frac{N_q \times D_q}{\pi \times D_m \times F_c \times Z} \times \arctan \left(Z \times \tan \left(\frac{\pi \times (F_q - F_c)}{F_q} \right) \right) \quad (3.1)$$

Where the crystal constant $N_q = 1.668 \times 10^{13} \text{ Hz/m}^{-10}$

density of quartz $D_q = 2.648 \text{ gm/cm}^3$

T_f = The thickness of the deposited material

F_q = the beginning quartz frequency

F_c = the ending quartz frequency

D_m = density of the deposited material

Z = Z-factor of the deposited material

3.1.2 Tooling Factor

Tooling Factor adjusts for the difference in material deposited on the quartz sensor versus the substrate. Tooling may be less than or greater than 100% as shown below:

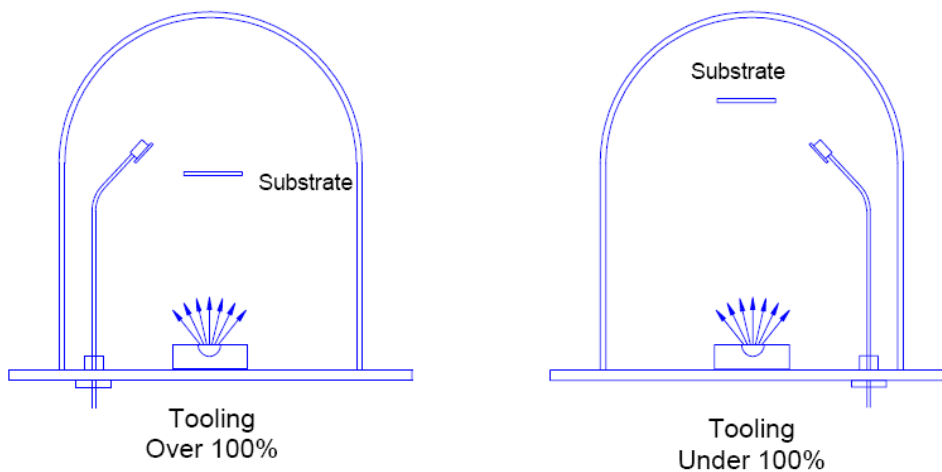


Fig. 3.1. The illustration of a simple deposition system. The heating source is at the bottom, and the sensor is shown in two different settings. (image from Sigma Instrument FAQs <http://www.sig-inst.com/faqpage.htm>)

To determine the tooling factor for the material one wants to evaporate, the standard procedure is as follows:

1. Place the substrate and a new quartz sensor in their normal position.
2. Set Tooling to an approximate value; Set Density and Z-Factor for your material.
3. Deposit approximately 100 to 500 Å of material.
4. Use a profilometer or interferometer to measure the substrate's film thickness.
5. The correct Tooling Factor is calculated by:

$$Tooling_{actual} = Tooling_{approx} \times \frac{Thickness_{actual}}{Thickness_{QCM}}, \quad (3.2)$$

where $Thickness_{QCM}$ denotes the thickness reading from deposition monitor using a method of QCM. $Tooling_{approx}$ is the tooling factor that you chose in the step 2.

$Thickness_{actual}$ is the thickness obtained in the step 4. $Tooling_{actual}$ is the tooling factor we want for this specific material evaporated by this specific facility.

3.1.3 Z-Factor:

Z-Factor is a ratio of the acoustic impedances of two materials. It is used to match the acoustic impedance of the deposited material (Z_m) to that of the base quartz sensor material ($Z_q=8.83$):

$$Z = \frac{Z_q}{Z_m} \quad (3.3)$$

For example, the acoustic impedance of gold is $Z=23.18$,

therefore the Z-Factor of Gold = $8.83 / 23.18 = 0.381$

Calculation of Z-Factor

Z-Factor can also be calculated using the Shear Modulus of quartz (U_q) and the deposited material (U_m):

$$Z = \sqrt{\frac{D_q \times U_q}{D_m \times U_m}} \quad (3.4)$$

where $U_q \sim 32\text{Gpa}$, D_q and D_m denote the density of quartz and deposited material separately.

Experimental Determination of Z-Factor

Unfortunately, Z-Factor and Shear Modulus are not readily available for many materials.

Therefore Z-Factors can also be determined empirically using the following method:

1. Deposit material until crystal life is near 50%, or near the end of life, whichever is sooner.
2. Place a new substrate adjacent to the used quartz sensor.
3. Set QCM Density to the calibrated value; Tooling to 100%.
4. Deposit approximately 1000 to 5000 Å of material on the substrate.
5. Use a profilometer or interferometer to measure the actual substrate film thickness.
6. Adjust the Z-Factor of the instrument until the correct thickness reading is shown.

Fortunately, the Z-Factor does not affect the accuracy of thickness measurement greatly if crystals are changed frequently. Fig. 3.2 shows the % Error in Rate/Thickness from using the wrong Z-Factor. For a crystal with 90% life, the error is negligible for even large errors in the programmed versus actual Z-Factor.

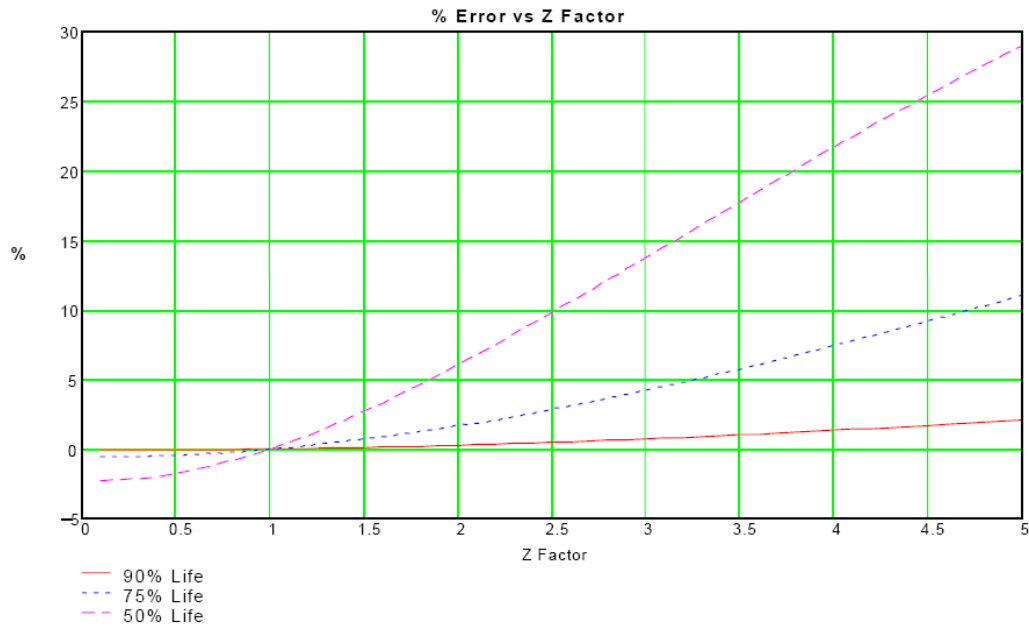


Fig. 3.2. The % Error in Rate/Thickness from using the wrong Z-Factor. This shows at 90% life of the sensor crystal, the error is negligible within a wide range of Z-Factor. (image from Sigma Instrument FAQs <http://www.sig-inst.com/faqpage.htm>)

3.1.4 Unknown materials

If the film density and Z-Factor of an evaporated material is known, as the tooling factor is fixed when using the same system, the QCM equation (3.1) can be applied directly to

determine the thickness of the film. However, most of the organic materials used in OLEDs have no film density information or Z-Factor determined. In this case, one can only set their value to be 1 and calibrate the 3rd parameter, the tooling factor, for each of the material. This is called the ‘effective tooling factor.’ To do so, another film-thickness determination technique other than QCM is needed to be explored.

3.2 Film Thickness Detection by Interferometry

The Thin-Film analyzer F-20 is a spectral reflectivity system that is PC-based and integrates measurement and analysis software with the spectrophotometer and fiber optic measurement hardware. The system is capable of modeling complex multilayer thin films.

3.2.1 Theory

In the case of a thin film on the surface of another material, both the top and bottom surfaces of the film reflect light, with the total amount reflected being dependent upon the sum of these two reflections. Furthermore, these two reflections may add together constructively or destructively depending upon their phase relationship. This phenomenon is due to the wavelike nature of light, with the phase relationship determined by the difference in optical path lengths of the two reflections.

The resulting interference pattern (interference fringes) can be used to determine the thickness of the film in question, assuming that refractive index and angle of incidence are both known. Conversely, refractive index can be determined if film thickness is known. Film thickness can thus be calculated using the following equation:

$$d = \frac{m}{2D_n \sqrt{n^2 - \sin^2 \theta}} \quad (3.5)$$

Where: d = film thickness

m = number of fringes in wavenumber region used

n = refractive index

θ = angle of incidence

D_n = wavenumber region used ($\nu_1 - \nu_2$; cm^{-1})

3.2.2 Detecting Steps:

1. Evaporating the unknown material on 2 Si substrates to 2 different prospective thickness, marked as film A and film B, with the following parameter: (Density, Z-factor, Tooling factor) = (1, 1, System tooling factor.)
2. Using the F-20 system to determine the real thickness of film A by measuring the reflecting light interference.
3. To do so, one needs to also know about the material's refractive and absorption index. But neither is known.
4. Set the thickness to be the initial setting value. Use physical model to fit the interference profile by adjusting refractive and absorption indexes to obtain the best fitting mathematically.
5. Using the Optical index thus found, determine the thickness of the film B.

6. Comparing this new thickness of film B with the prospective thickness by using equation 1.1 to obtain the ‘effective tooling factor’.
7. Using the new ‘effective tooling factor’ to evaporate another 2 films again with 2 different thicknesses.
8. Once again measuring the real thickness by F-20
9. Keep repeating steps 4-8 until the thickness measured by F-20 is equal to the thickness setting to be evaporated.

The ‘effective tooling factor’ needs to be determined for every new material.

3.3 The Fabrication of the Reference OLED Device

The steps previously described in 3.2.2 are actually the KEY to fabricate OLED devices. If they are followed incorrectly, the thickness of the device will be random, especially when co-evaporating two or more materials, the performance of such device is very sensitively affected by their concentration. To commission our OLED evaporator, an old-fashioned bi-layer OLED device¹ was fabricated. The energy diagram of such a device is shown in Fig. 3.3. The free holes and electrons are injected into the device and accumulated at the interface of ETL and HTL until they meet each other to form the excitons and recombine to emit light²⁻³.

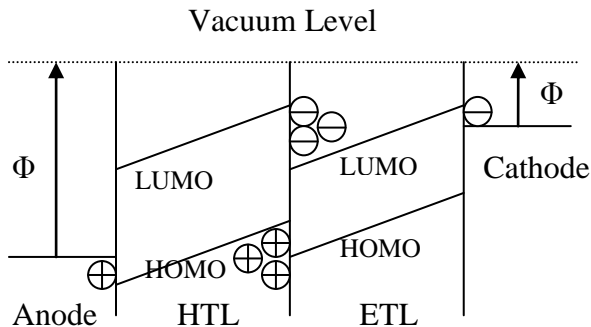


Fig. 3.3. The energy diagram of an OLED device with small molecule bi-layers sandwiched by two electrodes under applied bias. Electrons and holes are accumulated at the interface between HTL and ETL to form the excitons and later recombine to generate photons.

In OLED devices, the most commonly used anode which is pre-coated on the glass substrate is ITO. ITO is a mixture of indium(III) oxide (In_2O_3) and tin(IV) oxide (SnO_2), typically 90% In_2O_3 , 10% SnO_2 by weight. The fact that a 100 nm thick ITO thin-film not only can provide good electrical conductivity and optical transparency, but also a good energy level match with most hole-transporting small molecules' HOMO level⁴⁻⁵, makes it the favourite anode material for OLED devices. However the major problem of ITO is the roughness of the surface. The spikes formed during fabrication can be as rough as 30 nm⁶. Because the OLED devices usually are merely 100nm thick, this size of spikes has already been proved to have a huge effect on the morphology of the surface⁷, the electrical characteristics and luminescence life time. That is why the first layer deposited on the ITO must be thick, usually 40 nm, in order to cover the ITO spikes. But if one

want to make a thinner device (less than 100 nm.) a replacement material is still needed to be developed.

3.3.1 The fabrication:

The ITO coated glass substrate is cut to the size one needs, and the pattern of ITO is etched according to our design for the anode. And the step by step fabrication procedure is as follows:

1. Clean the ITO/Glass with chemical cleaning steps in an ultrasonic bath in detergent (to remove oil), deionized water (to remove the detergent), acetone (to remove most of the chemical contaminants), and isopropanol.
2. Then the devices undergo a pre treatment of UV-Ozone for 5 min. This treatment is believed to further lower the work function of ITO to 5.1 eV⁸. The following OLED device structures were then evaporated onto the substrates:
50 nm N,N'-bis(naphthalen-1-yl)-N,N'-bis(phenyl)benzidine (NPB), and 50 nm tris-(8-hydroxyquinoline) aluminum (Alq₃), evaporated in sequence.
3. 0.8 nm of lithium fluoride and 50 nm of aluminum were finally deposited at the rate of 1.5 Å/s as the cathode. The whole process is operated in a high vacuum of 2×10^{-7} mbar in a Lesker Spectros II Deposition System

3.3.2 Result and summary

The JV curve (Fig.3.4) shows a typical characteristic for a diode. The turn-on voltage is about 2 V, which also matches the maximum EL energy at about 2 eV as shown in Fig. 3.6. The current saturates after a sharp increase beyond the turn-on point due to the low charge carrier mobility of the small molecule thin-films. The electrons and holes accumulate at the interface of Alq₃ and NPB to form the excitons and recombine in the Alq₃ layer to generate green light (Fig 3.5.) This means the EL brightness should be proportional to the number of excitations recombined in the device per unit volume, which is proportional the number of charge carriers injected into the device, in other word, the current density. The phenomenon can be seen in Fig 3.6. The curve of current efficiency against the current density is shown in Fig 3.7. It reaches the maximum value of 2.2 cd/A and then gradually decreases because of aging.

The green emitting bi-layer OLED device was thus successfully fabricated with the brightness 550 cd/m² at 8V with efficiency 2.2 cd/A (Fig 3.8. and Fig 3.9.), which is comparable with the value reported based on similar device structure⁸. With the facilities carefully calibrated, the technology of fabricating a nano-scaled OLED device will be introduced in the next chapter.

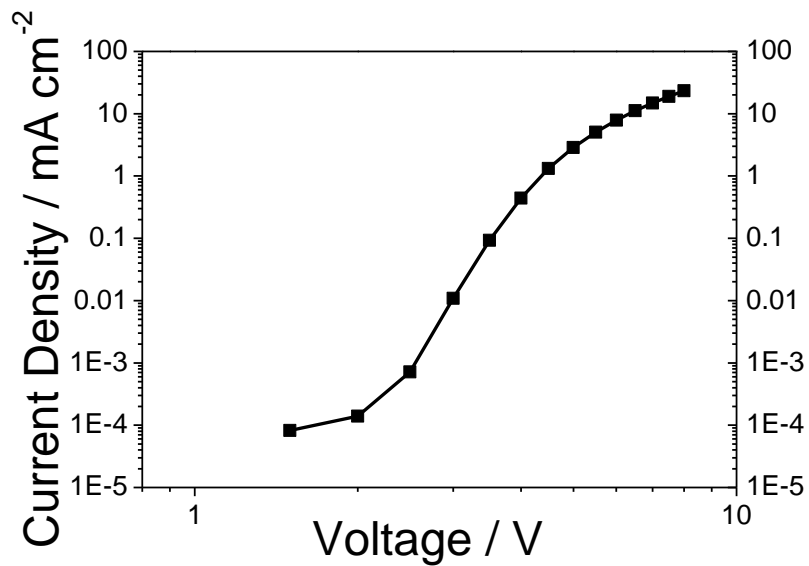


Fig. 3.4. The current density vs. applied voltage of the OLED device.

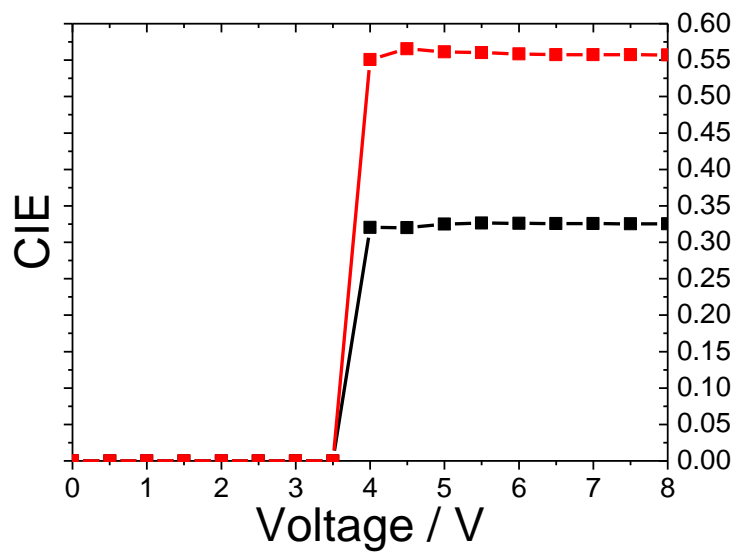


Fig. 3.5. The EL spectrum of the device with Alq₃ as the emitter.

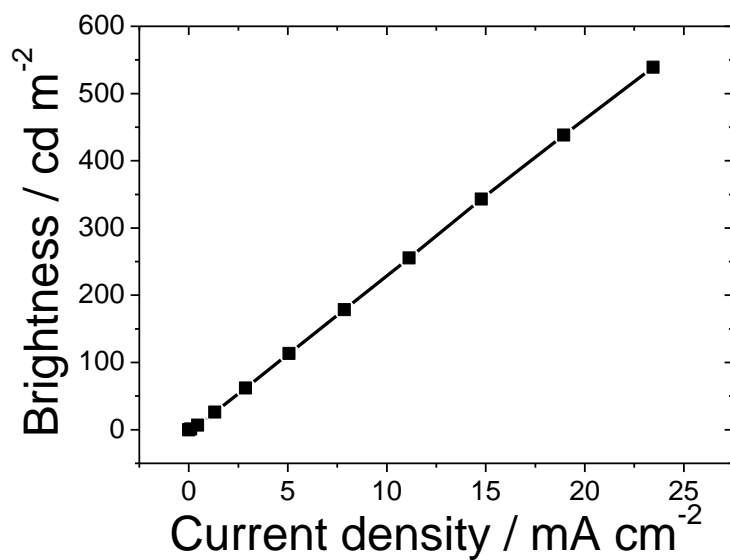


Fig. 3.6. The brightness against current density of the OLED device.

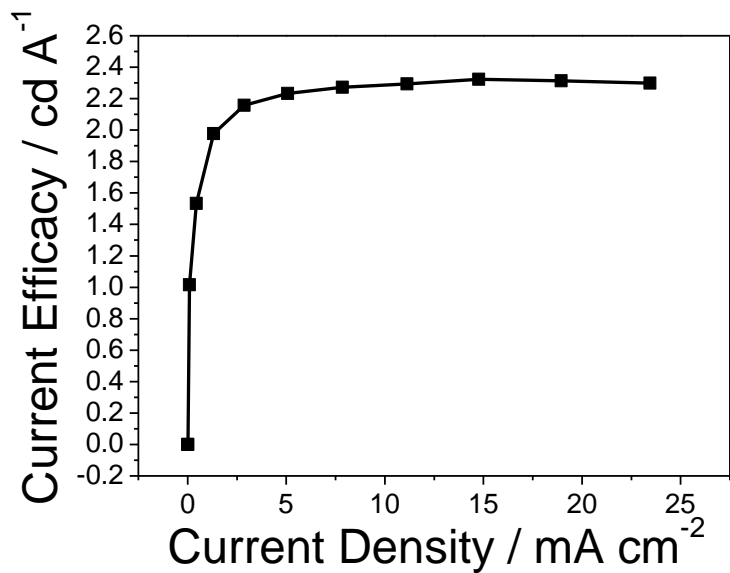


Fig. 3.7. The current efficiency against the current density of the OLED device.



Fig. 3.8. The completed OLED device with 4 big (5 mm x 8 mm) and 4 small (3 mm x 3 mm) pixels.

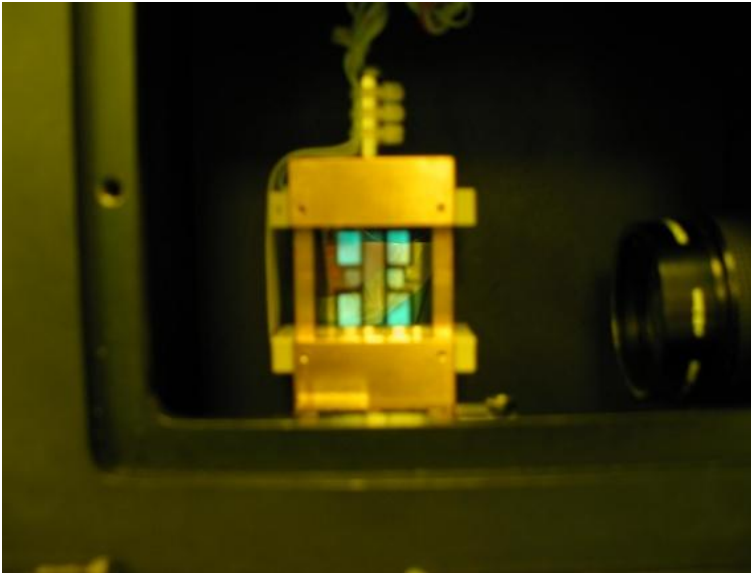


Fig. 3.9. The green-emitting bi-layer OLED device.

References:

1. J. Chan, A. W. Lu, C. H. Cheung, A. M. C. Ng, A. B. Djuricic, Y. T. Yeow and A. D. Rakic, presented at the Conference on Microelectronics - Design, Technology and Packaging II, Brisbane, AUSTRALIA, 2005 (unpublished).
2. H. Houili, E. Tutis, H. Lutjens, M. N. Bussac and L. Zuppiroli, *Comput. Phys. Commun.* **156** (1), 108-122 (2003).
3. C. W. T. a. S. A. VANSLYKE, *Applied Physics Letters* **51** (12), 913-915 (1987).
4. W. K. C. S.K. So, C.H. Cheng, L.M. Leung and C.F. Kwong, *Applied Physics A* **68**, 447-450 (1999).
5. Y. Park, V. Choong, Y. Gao, B. R. Hsieh and C. W. Tang, *Applied Physics Letters* **68** (19), 2699-2701 (1996).
6. Y. H. T. a. Y. S. H. e. a. K. B. Kim, *Japanese Journal of Applied Physics Part 2-letters* **42** (4B), L438-L440 (2003).
7. A. I. O. a. V. S. e. a. R. Castro-Rodriguez, *Applied Surface Science* **161** (3-4), 340-346 (2000).
8. F. Zhang, A. Petr, U. Kirbach and L. Dunsch, *Journal of Materials Chemistry* **13** (2), 265-267 (2003).

Chapter 4

Phosphorescent Organic Light-Emitting Nano Diodes

4.1 Introduction

The applications of nano-scale light sources are abundant, such as near-field scanning optical microscopy,¹ nano-photolithography,² quantum-communication which require single photon emitters,³ and biosensors.⁴ However the progress of miniaturizing such optoelectronic components by using inorganic LEDs based on GaAs, InAs and GaN is difficult, as below the scale of 100 nm the band structure becomes size sensitive to lattice strain, particle shape uniformity,⁵ surface defects,⁶ and compositional uniformity⁷ which change the materials optoelectronic properties. Organic LEDs, on the other hand, emit through individual molecules which means that there is less difference between macro- and nano- devices making them the potentially excellent materials for nano-scale light sources.⁸

In this chapter the fabrication of nano OLED⁹ based on a large density of isolated, consistently structured, randomly distributed nanodiodes is reported. To do this, an insulating, transparent, low refractive index template with track etched nanopores need to be used as a shadow mask to evaporate OLEDs on the ITO/glass. In these nanopores, there will be individual cylinder-shaped OLEDs with about 100 nm in diameter and 100 nm in length. But for the whole macroscopic device, this introduces an alternative optical design for an OLED as well. Now that the nano light emitting layers are isolated by lower

refractive index material, total refraction at the organic-insulator interface may be reduced by optimizing the dimension of the pores¹⁰.

4.2 Fabrication and Experiment

The fabrication of nanotemplate is as follows.¹⁰⁻¹¹ A 160 nm thick polycarbonate (PC) film was spin-coated on the 90 cm x 80cm ITO/glass substrate. The substrate then was treated with energetic heavy-ion irradiation. Finally, the etching process was performed in successive temperature-regulated baths filled with hydrogen peroxide to open the 50 nm radius holes with a density of $10^9/\text{cm}^2$. At this step, the thickness of the PC film decreased by 50 nm which means the depth of the pores becomed 110 nm. The pore diameter and density were determined by digital scanning electron microscopy (SEM).

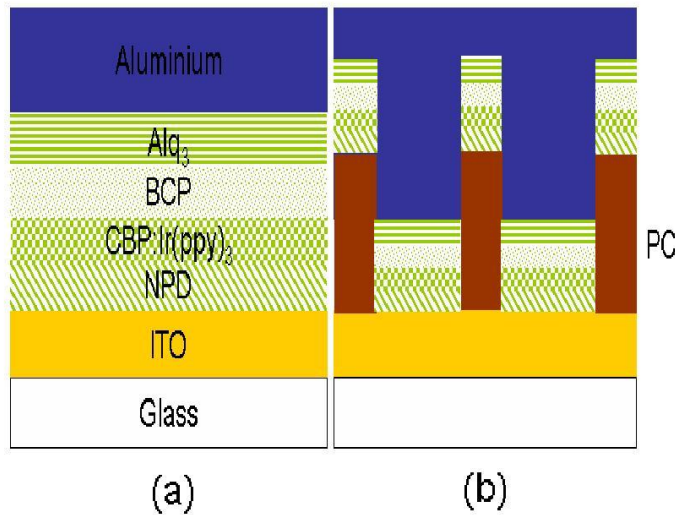


Fig. 4.1. Schematic view of the reference device (a) and the Nanotemplate device (b).

Two different kinds of substrates as shown in Fig.4.1 were studied: the device (a) is the reference with plain ITO glass, and the device (b) is the nanopores PC/ITO composite substrate. Only reference devices went through successive chemical cleaning steps in an ultrasonic bath in detergent, deionized water, acetone, and isopropanol. Both sets of devices underwent the pre treatment of UV-Ozone for 5 min.¹² as described in the Chapter 2. The OLED device structures were then evaporated onto the substrates: 40 nm N,N'-Bis(naphthalen-1-yl)-N,N'-bis(phenyl)benzidine (NPB), 20 nm CBP: 12% Tris[2-(2-pyridinyl)phenyl-C,N]-iridium; Tris(2-phenylpyridine) iridium (III) (Ir(ppy)₃), 6 nm 2,9-dimethyl-4,7-diphenyl-1,10-phenanthroline (BCP), and 20 nm Tris-(8-hydroxyquinoline) aluminum (Alq₃), evaporated in sequence.¹³ 160 nm of aluminum was finally deposited at the rate of 1.5 Å/s as the cathode. The whole process was operated in a high vacuum of 2×10^{-7} mbar in a Lesker Spectros II Deposition System.

4.3 Result and Discussion

The atomic force microscopy (AFM) image (Fig.4.2) shows the surface of the nanopore device after all the organic layers are evaporated before capping with the cathode. The organic layer surface is very smooth with only 7 nm of roughness, which is much smoother than the plain ITO surface.¹⁴ The nanopores in the image have a diameter about 110 nm, spread on the surface with about the same density as that of the nanotemplate which is $10^9/\text{cm}^2$.

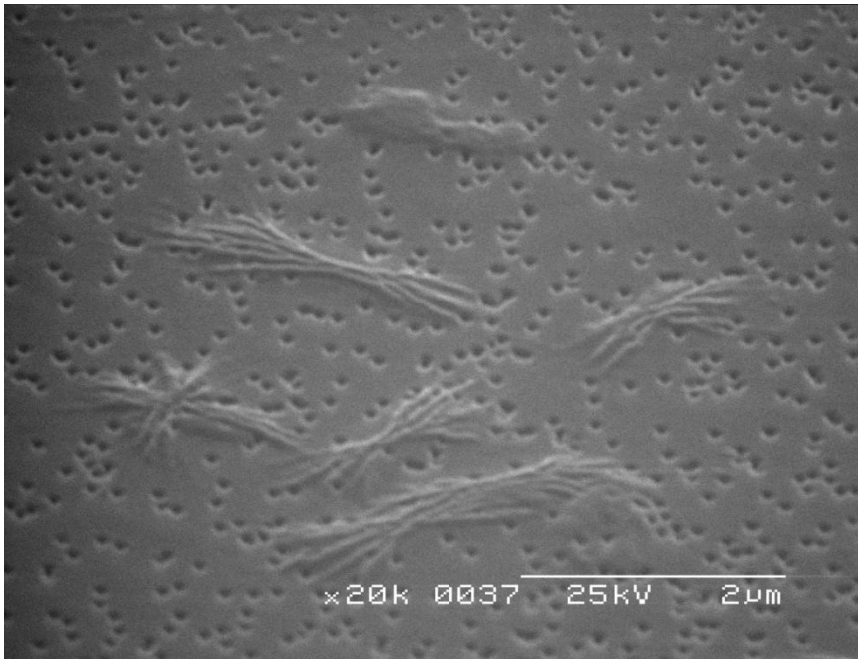
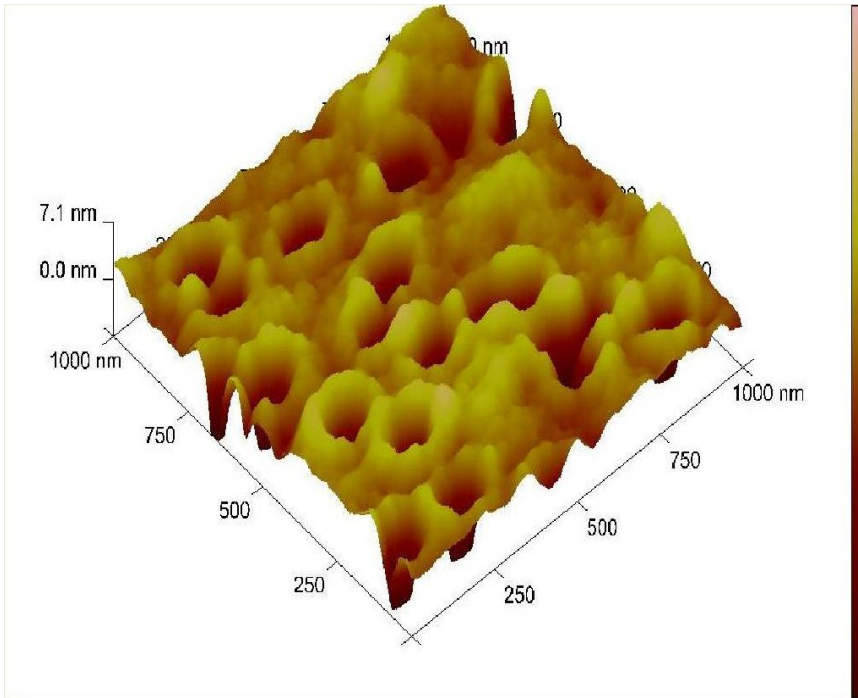


Fig. 4.2. Atomic force microscope (AFM) image (upper) and Scanning electron microscope (SEM) image (lower) for the surface of the nanopore device after all the organic layers are evaporated but before capping the cathode. The diameter of these pores are 110 nm each with a density of $10^9/\text{cm}^2$.

This figure suggests that the nanopore device had formed the same structure as the device (b) shown in Fig.4.1 only that the depth measurement of these pores is limited by the detecting AFM tip size, the true aspect ratio can be higher. Furthermore, after dissolving the polycarbonate layer on one of the nanopore devices, these nano cylinders OLEDs were observed by SEM. They stand on the ITO substrate as shown in Fig.4.3, which further proves they were bound on ITO very well.

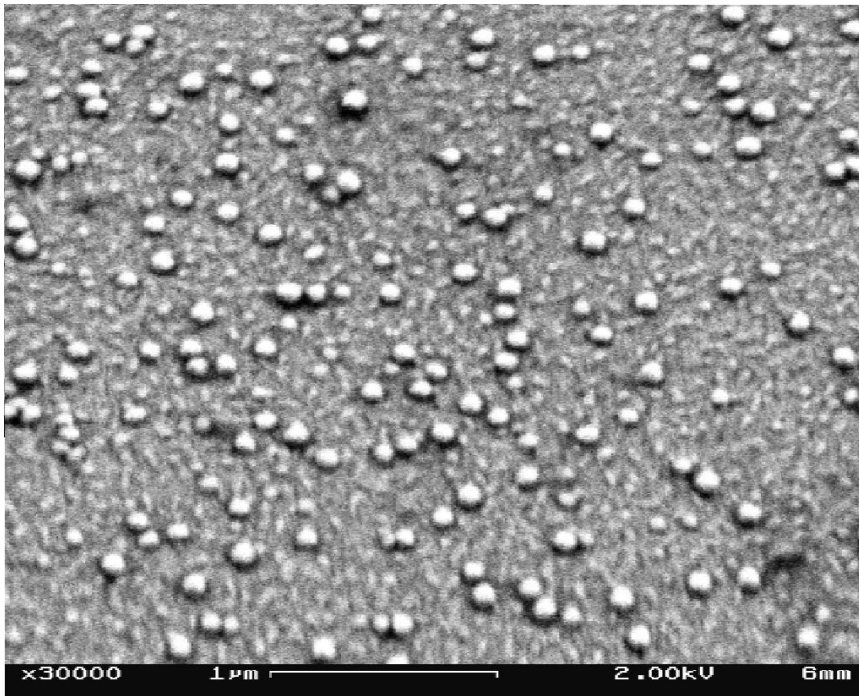


Fig. 4.3. Scanning electron microscope (SEM) image for the nanopore device after dissolving the polycarbonate layer matrix showing the cylindrical nano OLEDs left on the ITO substrate. The shadow shows their 3-D nature.

Although the distribution is random, they have relatively regular structures: all of them are still featuring 110 nm diameters. To complete device fabrication, aluminium was finally deposited. Aluminium will always form clusters during evaporation. However the aluminium surface of the nanopore device is much more homogeneous and flat than on the reference device, which had been observed with SEM as well. This may due to the ultra-smooth skin of the nanopore device as mentioned earlier.

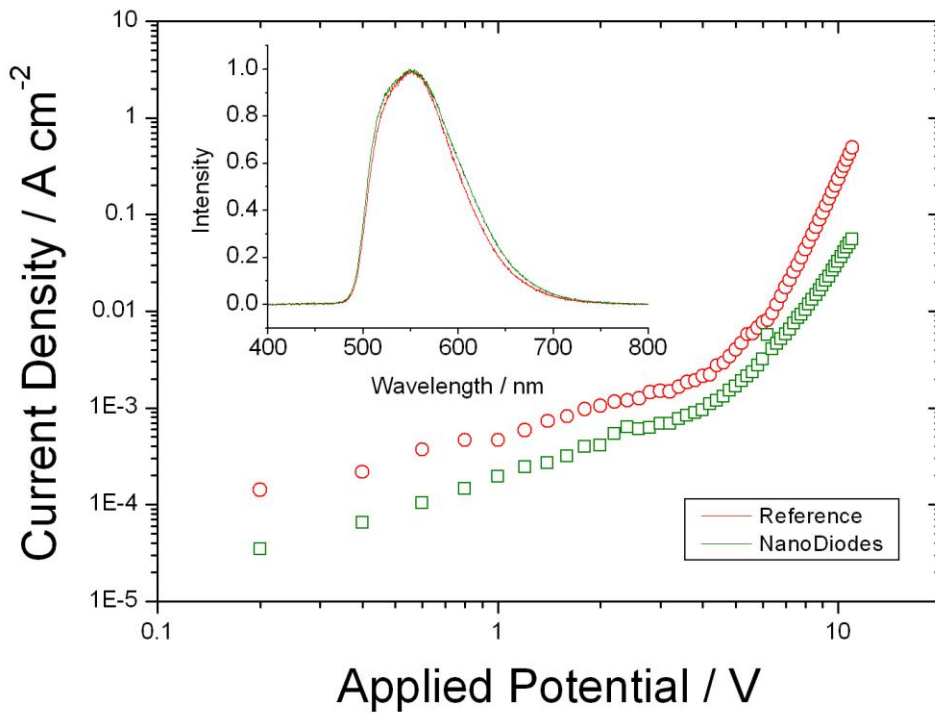


Fig. 4.4. Comparison of the I-V characteristic of the reference (The red line and red open circle) and the nanopore (The green line and green open square) device as indicated. The inset depicts the corresponding EL emission spectra.

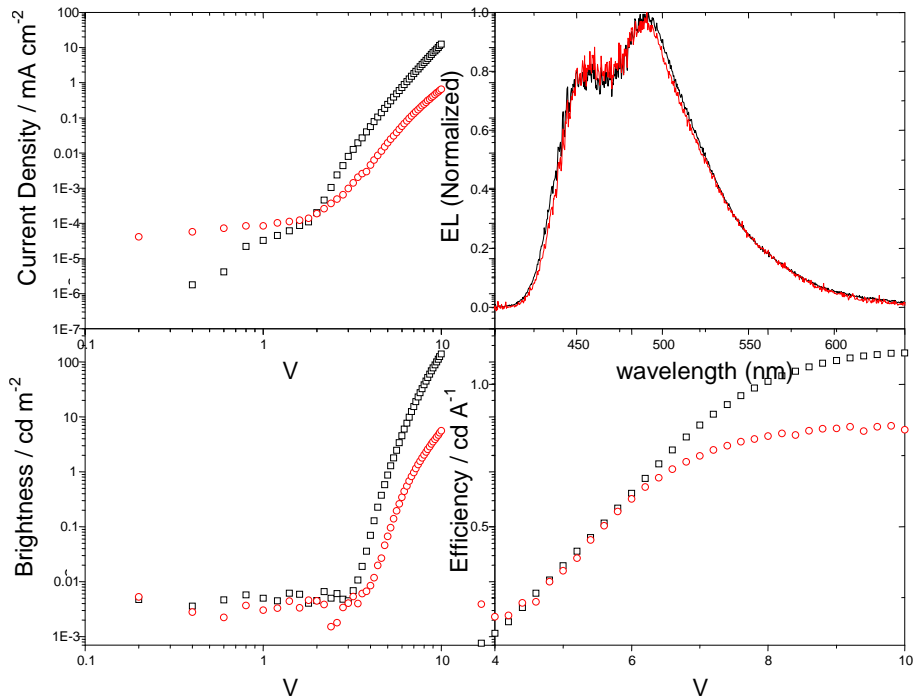


Fig. 4.5. Diagram of the I-V characteristic, brightness, efficiency, and EL spectrum of the reference (black) and the nanopore (red) devices based on spin-coated Spiro-TAD (blue emitter). The recipe is ITO/ poly(3,4-ethylenedioxythiophene) poly(styrenesulfonate) (PEDOT) / Spiro-TAD/ aluminium. These sets of experiments were performed as a comparison of spin coated and evaporated nanodiodes. It shows a similar result with the evaporated one: the nanodiode has lower brightness and lower efficiency, but has the same EL spectrum as the conventional device.

The electrical characteristic and EL spectrum of our devices were finally measured and the results are shown in Fig.4.4. The current density for the reference device (a) is about 1 order of magnitude larger than nanopore device (b). This is reasonable because the latter is only conductive through the nanopores, and the cross-sectional area is only about 10% of the device for a diameter of 110 nm at $10^9/\text{cm}^2$. Secondly, the almost parallel IV characteristic and similar turn on voltage suggest that the organic light emitting layer built in the nanopores behave no differently from directly deposited on the ITO layer. The injecting condition for these nanodiodes remains unchanged from its large area counterpart structure as well.

EL spectra show both device types to have a maximum emission at 550 nm. The red shift from the original Ir(ppy)₃ EL spectrum, which is about 510 nm,¹⁵ is due to heavy doping. At 1000 cd/m², the drive voltage, luminescence efficiency and power efficiency are 11.2 V, 16.17 cd/A, 4.53 lm/W for reference device (a) and 16 V, 12.12 cd/A, 2.38 lm/W for nanodiodes device (b). There are three probable reasons for the performance of the nanodiodes device (b) being slightly lower compared to reference device (a). First, defects introduced at the interface between PC and organic layers, and once the nanotemplate is made, the substrate cannot be cleaned chemically as people did on ITO surface. Secondly, only 1/10 area of the pixel is active, in order to reach similar brightness the nanodiodes have to be driven harder which might deteriorate the efficiency. Thirdly, aluminium surface is formed by clusters during thermal evaporation, and the size of these grains can be from 10 nm to 200 nm¹⁶ and the diameter of our nanopores is merely 100 nm. There are, therefore, some nanodiodes fabricated without contacting the

cathode since the aluminium cluster is blocked outside the pores, thus as a whole decreases the luminescence performance.

Surprisingly, when driving both devices very hard at more than 2×10^6 V/cm, they decay in very different ways. The reference device gets very bright and begins to burn from the center of the pixel, then spreads out over the whole pixel in seconds. The nanopore device is not as bright, however the pixels begin to “sparkle”. Some areas then gradually stop glowing, but the whole device still works at those surviving diodes. These phenomena can be further understood by SEM. When high bias is applied on the device, something inside the nano-scale organic structures begins to degrade, and form many ‘bubbles’ on the aluminium surface as [Fig.2.5](#).

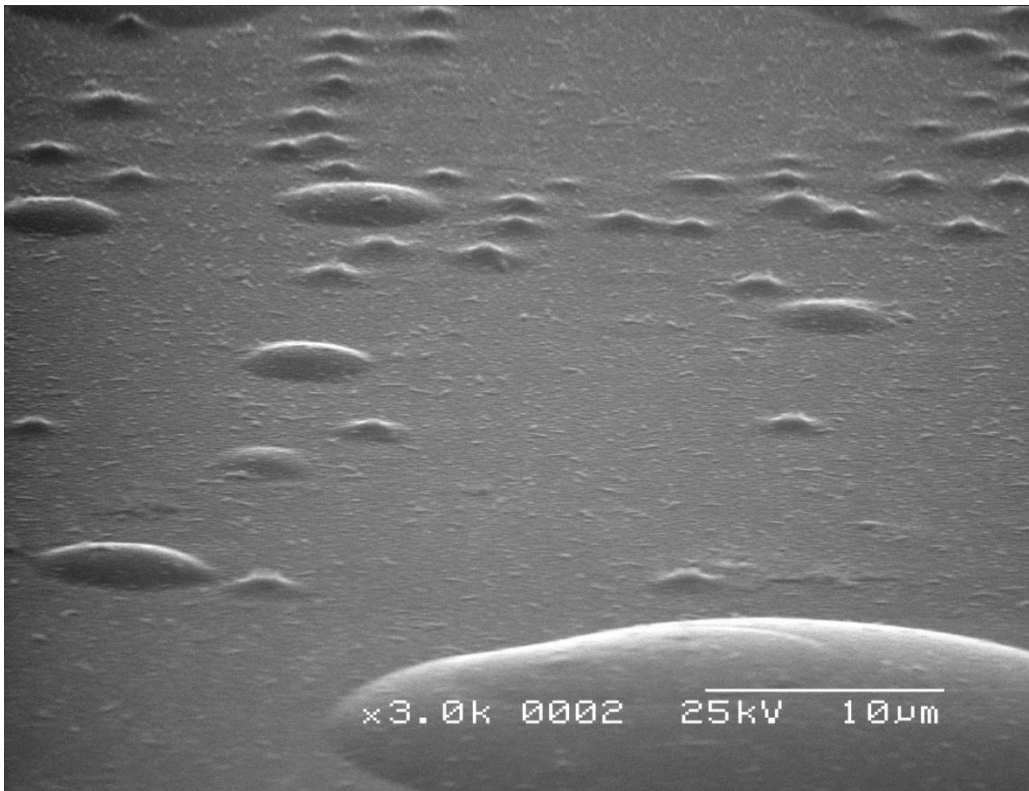


Fig. 4.6. The SEM image of the nanopore device after driving at 21V for several seconds.

The sizes of bubbles are very different. The one at the bottom is about $300 \mu\text{m}^2$ which probably covers 3000 nanopore diodes. The smaller one at the top can be as small as less than $1 \mu\text{m}^2$, which only covers one nanopore diode.



Fig. 4.7. The SEM image of the nanopore device after driving at 21V for several seconds.

It was measured on the other region of the same surface as in figure 4.6.

[Fig.4.6](#) shows the SEM image of the other area on this same device. These ‘volcano-like’ constructions are in size of $0.2 \mu\text{m}^2$ which about covers 1-2 nanodiodes only. These volcanoes are believed to be the eruption of bubbles in [Fig.4.6](#). This image shows how the nanotemplate structure isolates these decaying centres and protects the device from degradation ‘infection’.

In this case, the structure of the nanotemplate works like a watertight compartment to prevent the migration of degradation.¹⁷⁻¹⁸ These sparkling spots are very likely to be the individual nano-OLEDs. It is therefore proper to see the nanopore device as an assembly of separated nanodiodes. Although it would be dimmer when some diodes have burned, the whole device does not all fail catastrophically. This shows a promising character to increase the working time of OLED devices.

4.4 Summary

The method to fabricate phosphorescent Organic Light-emitting nano diodes based on Ir(ppy)₃ through a PC nanotemplate with high consistency and stability structured nanopores which featuring 110 nm diameter has been reported. The emission properties and electrical character are both comparable to the large area reference device. It also directs a probable way to increase device lifetime from its design by isolating each emitting diode. Instead of aluminium, other metals can be used as cathodes to have a better contact with the organic layer buried in the nanopores. Different diameters of nanotemplates can also be made in the future in order to see the possible microcavity effect.¹⁹

References:

1. M. Chaigneau, G. Ollivier, T. Minea and G. Louarn, Review of Scientific Instruments **77** (10) (2006).
2. F. A. Boroumand, P. W. Fry and D. G. Lidzey, Nano Letters **5** (1), 67-71 (2005).
3. Y. Yamamoto, Quantum Information Processing **5** (5), 299-311 (2006).
4. R. Popovtzer, T. Neufeld, E. Z. Ron, J. Rishpon and Y. Shacham-Diamand, Sensors and Actuators B-Chemical **119** (2), 664-672 (2006).
5. J. Zou, X. Z. Liao, D. J. H. Cockayne and R. Leon, Physical Review B **59** (19), 12279-12282 (1999).
6. H. Temkin, G. J. Dolan, M. B. Panish and S. N. G. Chu, Applied Physics Letters **50** (7), 413-415 (1987).
7. W. D. Sheng and J. P. Leburton, Physical Review B **63** (16) (2001).
8. H. Yamamoto, J. Wilkinson, J. P. Long, K. Bussman, J. A. Christodoulides and Z. H. Kafafi, Nano Letters **5** (12), 2485-2488 (2005).
9. J. G. C. Veinot, H. Yan, S. M. Smith, J. Cui, Q. L. Huang and T. J. Marks, Nano Letters **2** (4), 333-335 (2002).
10. E. Ferain and R. Legras, Nuclear Instruments & Methods in Physics Research Section B-Beam Interactions with Materials and Atoms **174** (1-2), 116-122 (2001).
11. E. Ferain and R. Legras, Nuclear Instruments & Methods in Physics Research Section B-Beam Interactions with Materials and Atoms **208**, 115-122 (2003).
12. S. K. So, W. K. Choi, C. H. Cheng, L. M. Leung and C. F. Kwong, Applied Physics a-Materials Science & Processing **68** (4), 447-450 (1999).
13. M. A. Baldo, S. Lamansky, P. E. Burrows, M. E. Thompson and S. R. Forrest, Applied Physics Letters **75** (1), 4-6 (1999).
14. S. Besbes, H. Ben Ouada, J. Davenas, L. Ponsonnet, N. Jaffrezic and P. Alcouffe, Materials Science & Engineering C-Biomimetic and Supramolecular Systems **26** (2-3), 505-510 (2006).
15. C. Rothe, S. King and A. P. Monkman, Physical Review B **73** (24) (2006).
16. R. B. Laibowitz, E. I. Alessandrini and G. Deutscher, Physical Review B **25** (4), 2965-2967 (1982).
17. S. C. Luo, H. H. Chung, E. T. Pashuck, E. P. Douglas and P. H. Holloway, Thin Solid Films **478** (1-2), 326-331 (2005).
18. S. F. Lim, W. Wang and S. J. Chua, Materials Science and Engineering B-Solid State Materials for Advanced Technology **85** (2-3), 154-159 (2001).
19. A. M. Adawi, A. Cadby, L. G. Connolly, W. C. Hung, R. Dean, A. Tahraoui, A. M. Fox, A. G. Cullis, D. Sanvitto, M. S. Skolnick and D. G. Lidzey, Advanced Materials **18** (6), 742-+ (2006).

Chapter 5

High Efficiency Charged Iridium Metal Complex Based Light-Emitting Diodes

5.1 Introduction

Currently, the potential of organic ELs is mainly exploited in terms of multilayer devices made of small organic molecules (OLEDs) and single layer devices employing polymers (Poly-LEDs). To date, OLEDs in general deliver better efficiency compared to their polymeric counterparts but they are more complex to produce. Mandatory to achieve high efficiency in both cases is the use of triplet emitters to exploit all excitons generated, which in turn requires host matrix materials that on the one hand allow for charge injection and transport and on the other possess a higher triplet energy than the guest dopant to confine the energy at the emitter¹⁻². For the simple Poly-LEDs where it is possible to directly print in air, such host materials suitable for blue emitters are not yet available³. This problem is solved in state-of-the-art OLEDs using a range of functionalizing layers, whose production thus requires a complex evaporation sequence. For decent electron injection, the single layer diodes further need a reactive metal cathode. But it is only a minor drawback, since for stable operation both kinds of organic diodes need thorough encapsulation anyway.

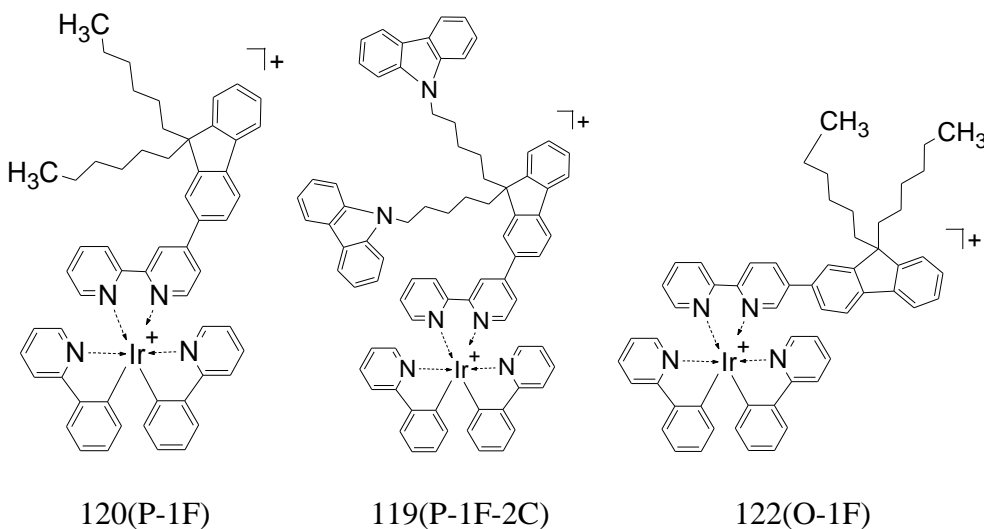
A few years ago, an alternative approach to organic EL, namely single compound Light emitting Cells (LECs), were successfully demonstrated⁴⁻⁵.

Here, the whole organic part of the diode consists of a single, spin coated layer of a cationic heavy metal complex only. These diodes are made entirely of heavy metal triplet emitter and as such harness all excitations created without the need of suitable host material. Such iridium complexes carry a positive charge, which is balanced by a small and mobile counter ion. Following ion drift after applying an external electrical field, charge injection is aided by the formation of ionic layers close to the electrode. The results are low turn-on voltages leading to high power efficiency without using reactive metals⁶⁻⁷. The effect is similar to the concept of doping the organic layer at the proximity of the metal interface with the type of charge to be injected⁸. In conclusion, without many efforts, LECs combine the best of the OLED and the polyLED approaches and as such warrant intensive research efforts in the coming years.

Questions to be solved include the fairly long turn on time which may be tackled sufficiently by employing smaller, more mobile counter ions or some kind of freeze-in of the space charge layer distribution after initially charging the diodes for example by using a cross linking matrix. The performance of the current generation of LECs may be further increased by controlling excitation migration, since mobile excitatons are prone to quenching at impurity sites (concentration quenching) or may reach the highly charged space charge layers at the electrodes leading again to non-radiative decay⁹. Finally, a better understanding of charge injection and transport mechanism is necessary to design a robust higher performance diode. Initially, the very low turn-on voltage was taken as an indication of pure ohmic injection, independent of choice of electrode material. However for equal pairs of electrodes the diode efficiency strongly depends on the driving

direction. These observations do suggest that the charge injection is not purely ohmic therefore the choice of electrodes can be important¹⁰.

To begin our work, 5 new iridium complexes as shown in Fig 5.1 were synthesized by Professor Martin Bryce's group of the chemistry department. These materials are classified into 2 families. Family 1 has ligands bonded with the carbon opposite to the nitrogen forming a parallel formation, labelled 120(P-1F) and 119(P-1F-2C). Family 2 has ligands bonded with the carbon next to the one using in last two samples and forming an orthogonal formation, labelled 122(O-1F), 99(O-2F) and 124(O-1F-2C). The reason for the different attached position of the fluorene ligand is to test whether this would alter the migrating behaviour of the charged counter ions. And species contains carbazoles in the structure such as 4,4'-bis(9-carbazolyl)-biphenyl (CBP)¹¹ usually has higher hole mobility¹². Therefore complex 119(P-1F-2C) and complex 124(O-1F-2C) are synthesized to hopefully give better charge carrier balance inside the devices.



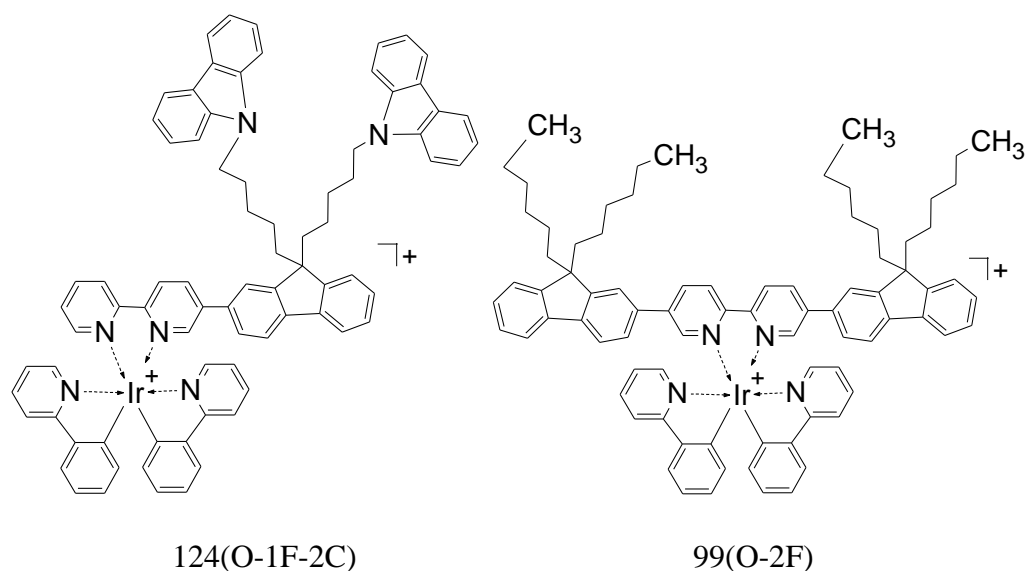


Fig. 5. 1 The structure of the charged iridium complexes studied in this thesis. The counter ion is always PF_6^- . They are classified into 2 families.

Family 1:

120(P-1F): P denotes parallel and 1F denotes 1 fluorene ligand.

119(P-1F-2C): 2C denotes 2 carbazole ligands.

Family 2:

122(O-1F): O denotes orthogonal.

124(O-1F-2C)

99(O-2F).

The process of LEC device fabrication is described in chapter 5.2. In chapter 5.3.1-5.3.3, different cathode materials and additional electron transporting material as listed in [table 5.1](#) are deposited to change the electron injection condition. In chapter 5.4, the effect of the attached functional ligands to the device performance is investigated. The triplet

lifetime of the charged Ir complex thin-films are reported in chapter 5.3.5. Finally in the chapter 5.3.6, an example of the EL performance of the best device in the study is presented.

Table 5.1

Device Label (what they are named when mentioned in this chapter)	Cathode Material(thickness/nm)	note
Al	aluminium(100)	Stable; Large injection energy barrier.
Ba	barium (1.5)/aluminium(100)	Unstable; Good injection energy level match
LiF	lithium fluoride(0.15)/aluminium(100)	Relatively stable; Good electron injection property.
Alq3	Alq3(10)/LiF(0.15)/Al(100)	Alq3 has good electron mobility.
BCP	BCP(7)/ Alq3(10)/LiF(0.15)/Al(100)	BCP block the holes and improve the charge carrier balance.

5.2 Experimental

5.2.1 Sample Preparation

1. All complexes were dissolved in acetonitrile at 30mg/ml (used 15 mg).
2. Stirred and heated at 50 °C until completed dissolved.
1. The ITO substrates (3 cm x 4 cm, 9 pixels) were put in an ultrasonic bath and cleaned in sequence in detergent, deionized water, acetone, and isoproponal and then exposed to UV-Ozone for 5 min.

2. Spin coated the Poly(3,4-ethylenedioxythiophene) poly(styrenesulfonate) (PEDOT) on the ITO substrates and heated at 70 °C for 4 hours.
3. The solution was spin coated with 5 s @ 400rpm and 60 s @ 2500rpm onto the preheated ITO substrates
4. The diodes were transferred to the Lesker Spec II evaporating chamber.
5. All metal cathodes were deposited under high vacuum of 2×10^{-6} mbar.
6. All devices were tested immediately after fabrication to avoid further degradation.

5.2.2 Analysis method

The two factors studied in this thesis are the effect of different ligand structures and different cathode materials. To avoid confusion, the analysis begins with comparing each Ir complex material based LEC devices with different cathodes as listed in [table 5.1](#). Al, LiF, and Ba devices are compared to see whether the work function of the electrode material is really unimportant as in previous reports¹³. A thin Alq₃ layer and BCP layer are inserted to provide easier electron transporting and hole blocking and to see if these functional layers improve the performance of LECs by having better charge carrier balance as they do in OLED devices.

Secondly, different complexes with fixed electrodes were compared in order to see what roles the different ligands play in the LEC devices performance. In order to keep this analysis simple, the single layer cathode devices, such as the Al, LiF, and Ba devices were explored.

The EL characterization facilities are as introduced in chapter 2.4.

5.3 Result and Discussion

5.3.1 Comparison of different cathode material with complexes in Family 1 as light

emitting layer

120 (P-1F)

Al vs. Ba/Al and LiF/Al

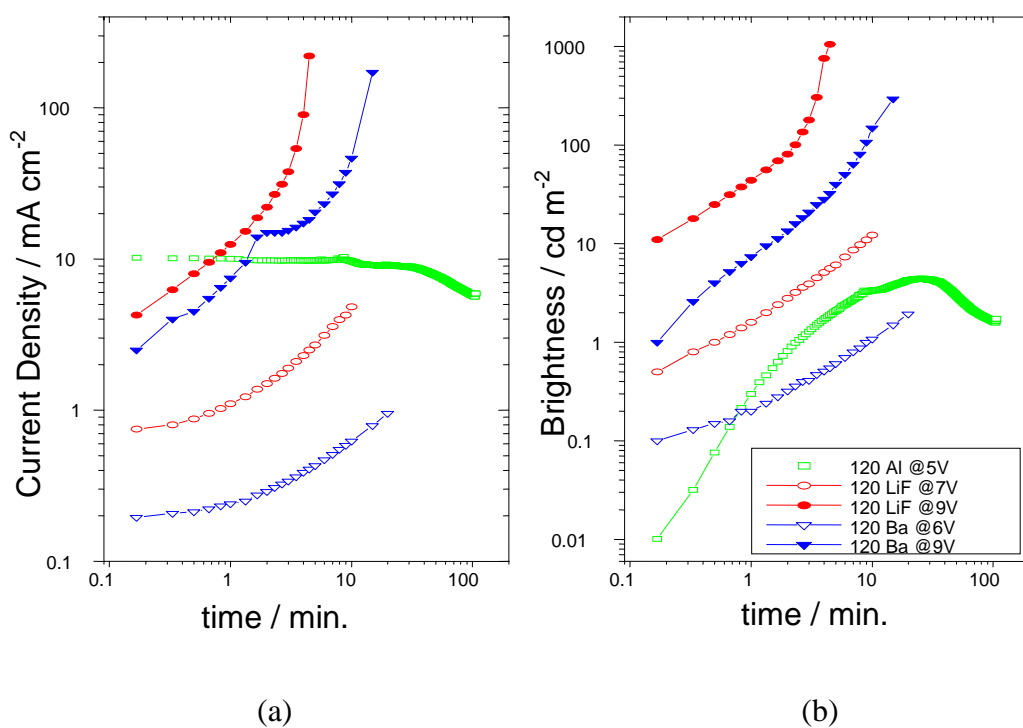


Fig. 5. 2 The current density and brightness against time for P-1F complex with Al (green), Ba (blue), and Al/LiF (red).

From the data it is readily seen that Al devices have very poor performance. The reason the devices performed so badly with such weak luminescence might be that it had its aluminum cathode evaporated 27 days later than the iridium complex had been spin-coated. The material might have degraded a lot, but it was kept in the 1×10^{-7} mbar vacuum chamber during the periods. Both high and low charging voltages were applied

to the LiF and Ba devices. The devices with the same electrode have larger current and a steeper increase of current in the first few minutes when they were driven harder. The LiF device charged at 9V reaches 1000 cd/m^2 after 4 minutes, and 100 cd/m^2 at 6V after 10 minutes, for example. The 3V difference has improved the brightness by a factor of 10. The Al device has a steady current during the charging cycle at 5V, however the brightness increases by a factor of 400 after 20 minutes. Both LiF and Ba layers have lower initial current at the beginning comparing to the Al devices, and require larger charging bias to emit light, but after about 1 minute with higher charging voltage applied, it was observe that the current has already surpassed the Al only device.

Although the brightness keeps increasing along with the current, the high current degrades the devices quickly after 4 minutes at 10^4 mA/cm^2 for LiF device as shown in Fig 5.3. It is also worth noticing that the effect of LiF buffer layer is that LiF devices show a lower current than Al device at 7V charging voltage, but are 4x brighter, which suggests the LiF layer can block the hole current and increase the electron injecting at the same time, giving a better balance of electron and hole current in the device.

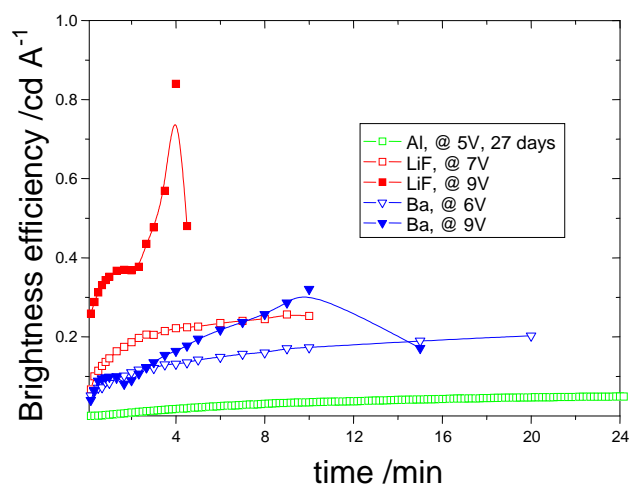


Fig. 5. 3 The luminescence efficiency against time for P-1F complex with Al (green), Ba (red), and Al/LiF (blue).

When charged for 4 minutes, the current density of LiF device increases by a factor of 3 for 7V and 21 for 9V; for the Ba device, 2 for 6V and 7 for 9V. This contributes to the improvement of efficiency by a factor of 3 for both LiF devices and 2.6 and 4.1 times respectively for Ba devices at 6V and 9V. Despite the increase of the efficiency they are all poor devices yielding less than 1 cd/A, which suggests a huge charge carrier imbalance in the device: i.e. a hole dominated device. The larger charging bias induces more injection of both electrons and holes. Since there are few electrons in the device at the beginning, the efficiency increases rapidly over the first few minutes then saturates afterwards. There seems to be two-steps of increase in both current density and efficiency at higher bias. The first increase of current brings the efficiency to an equilibrium state. The second step again increases current; this causes both efficiency and current to grow continuously until the current is too high and destroys the devices.

LiF/Al vs. Alq₃/LiF/Al and BCP/ Alq₃/LiF/Al

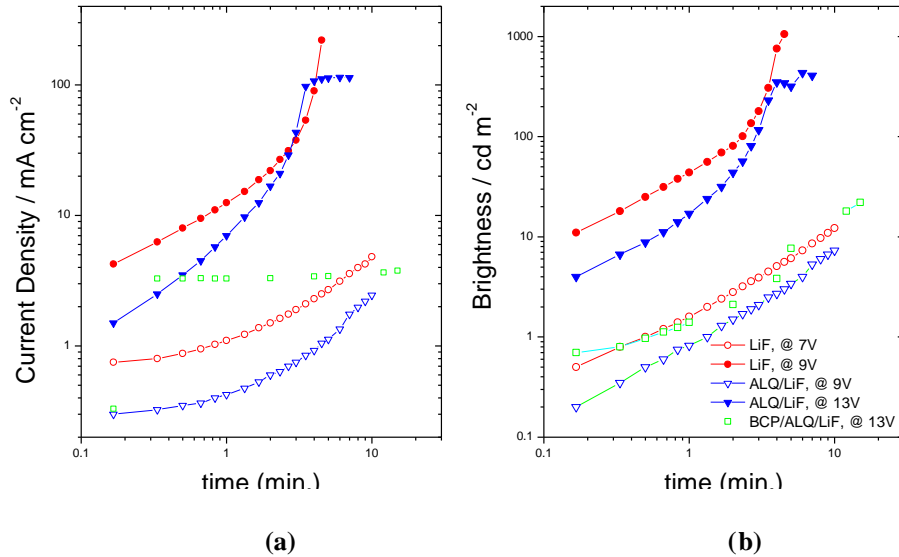


Fig. 5. 4 The current density and brightness against time for P-1F complex with Al/LiF (red), Al/LiF/ Alq₃ (blue), and Al/LiF/ Alq₃/BCP (green)

To improve electron injection and transport, additional Alq₃ and BCP layers are introduced. The most apparent effect of introducing these layers is that a larger driving voltage is required. In order to reach similar brightness as the single layer cathode devices, Alq₃ devices needed 4 V more for 1000cd/m², 2 V more for 10 cd/m², and 4V more for further additional BCP device to reach 10 cd/m². Despite this, there is a very similar behaviour of current and brightness against time between Alq₃ device at 9V and LiF device at 7V, Alq₃ device at 13V and LiF device at 9V. There seems to be 2 different kinds of mechanism at high voltage and low voltage.

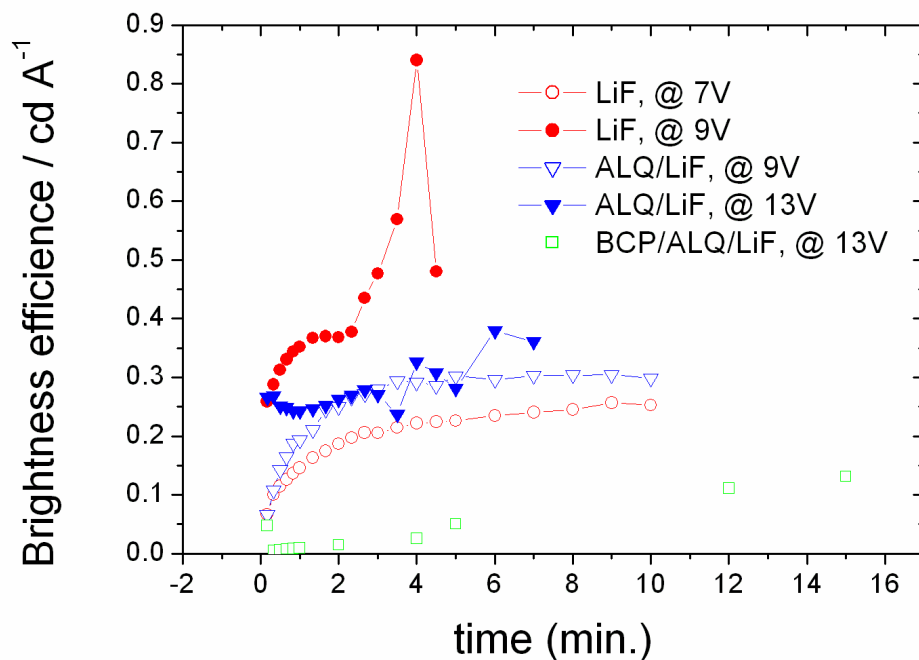


Fig. 5. 5 The luminescence efficiency against time for P-1F complex with Al/LiF (red), Al/LiF/ Alq₃ (blue), and Al/LiF/ Alq₃/BCP (green).

For these charged complex devices, it is the bias across the emitting layer that drives the ions to the metal/organic interface which influences the injecting barriers, and makes the benefit. The additional Alq₃ layer reduces the bias across the emitting layer, so it needs to be driven harder to produce the same bias across the iridium complex layer as a simple Al device.

Alq₃ devices have similar efficiency at 9V and 13V after 2 minutes of charging. They seem to reach the same equilibrium state in the emitting layer. The additional voltage is

likely to be dropped across on the Alq₃ layer. Also the Alq₃ layer, acts as a hole blocking layer, helps to prevent the current from continuous ramping.

119 (P-1F-2C)

Ba/Al vs. LiF/Al, Alq₃/LiF/Al, and BCP/ Alq₃/LiF/Al

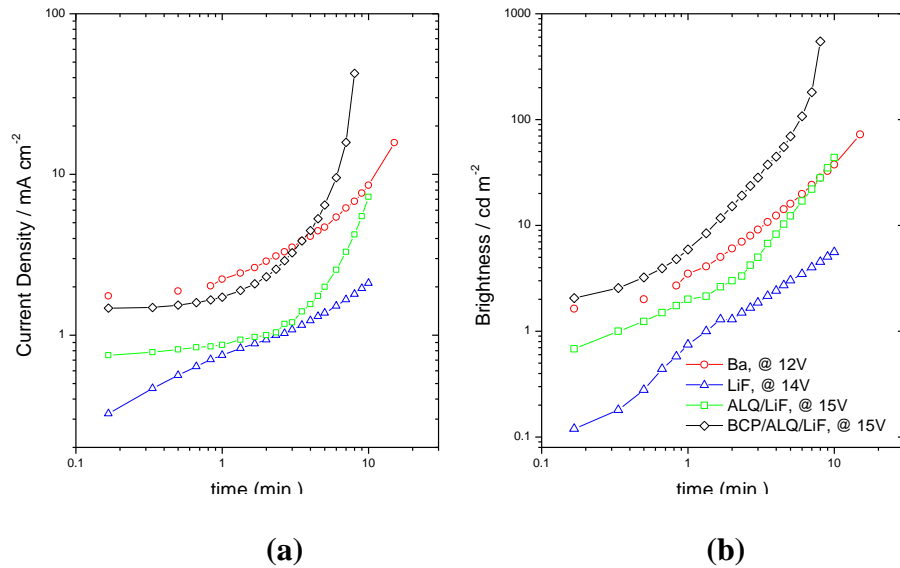


Fig. 5. 6 The current density and brightness against time for P-1F-2C complex with Ba (red), Al/LiF (blue), Alq₃/LiF/Al (green), and BCP/ Alq₃/LiF/Al (black).

The device characteristics again can be categorized into 2 groups: single layer cathode devices and multiple layer cathode devices: Ba and LiF devices have similar behaviour and so do Alq₃ and BCP devices.

The latter has an obvious ‘turn-on’ when charged for 3 minutes. This turn-on behaviour occurs when charging at higher voltage as well in [fig.5.4](#) for complex 120(P-1F).

Further, if regarding the current density at time zero as the ability of charge injection according to the original energy scheme, one can conclude that for the complex 119(P-1F-2C), Ba devices have better energy matching than LiF devices. While with insertion of Alq₃ and BCP layers (which again required larger driving voltage), the brightness reaches about 550 cd/m² after 8 mins of charging, although the initial current and brightness is very similar with Ba device. Furthermore, as the bias across the iridium complex layer in the BCP devices is the smallest among this comparing group, it takes a longer time for the counter ions in the iridium complex layer to migrate to the anode. However when the steady state is reached, the effect of increasing both electron and hole injection is large in line with the lower barrier. It increases the current by a factor of 30 and the brightness by 220 in 8 minutes. That is a 10 times improvement in efficiency.

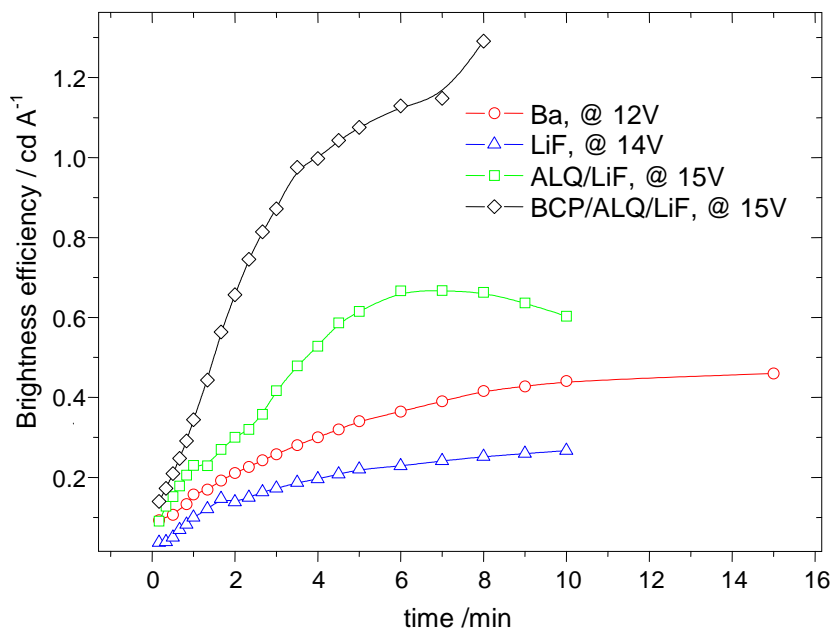


Fig. 5. 7 The Luminescence efficiency against time for P-1F-2C complex with Ba (red), Al/LiF (blue), Alq₃/LiF/Al (green), and BCP/ Alq₃/LiF/Al (black).

The earlier turn-on in BCP and Alq₃ devices also leads to better efficiency. This might come from better charge carrier balance since Ba and Alq₃ devices have similar brightness, but due to the hole blocking characteristic of Alq₃ the latter is twice as efficient as the former. This is further improved two fold in efficiency by BCP layer. But it is observed that both LiF and Ba devices maintain at their steady state once they reach equilibrium, and the Alq₃ device has a maximum in efficiency for 7 minutes of charging then gradually decays. This might be due to the interface defects between Alq₃ and LEC layers that trap electrons.

5.3.2 Comparison of different cathode material with complexes in Family 2 as light

emitting layer

122 (O-1F)

Al vs. Ba/Al and LiF/Al

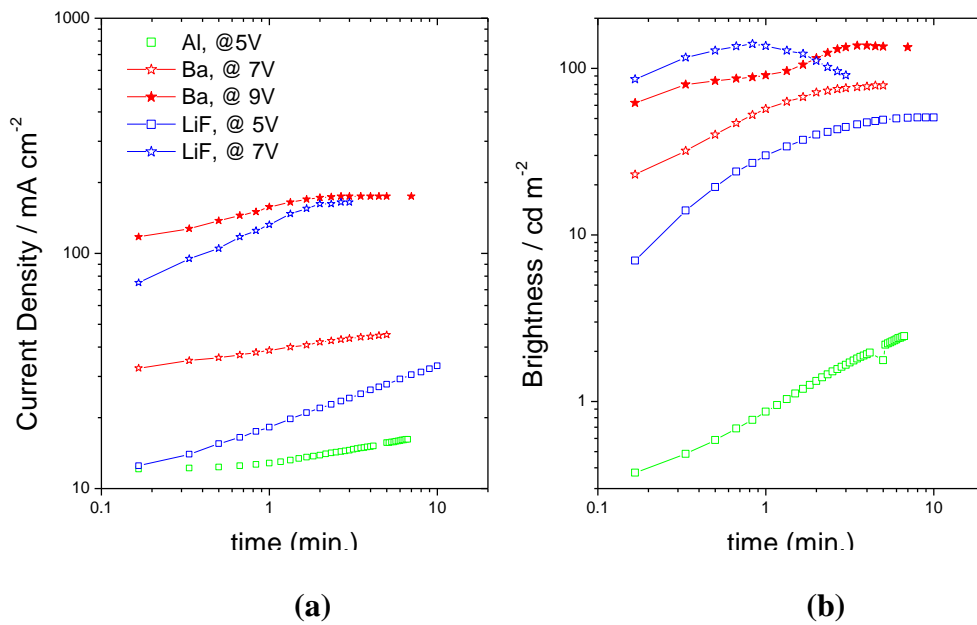


Fig. 5. 8 The current density (a) and brightness (b) against time for O-1F complex with Al (green), Ba (red), and Al/LiF (blue).

For complex 122(O-1F), the charging time for all the three cathodes according to Fig.5.8 (b) is very similar: about 2 minutes. The additional LiF layer, compared to the Al device, improves the current and brightness by a factor of 2 and 10 at 5V. At 7V the LiF device reaches 100 cd/m² within a minute but again degrades afterward due to the large hole

current. Although the Ba devices require higher driving voltage: 9V to get 100cd/m^2 , the device is quite stable even with the same current as LiF device.

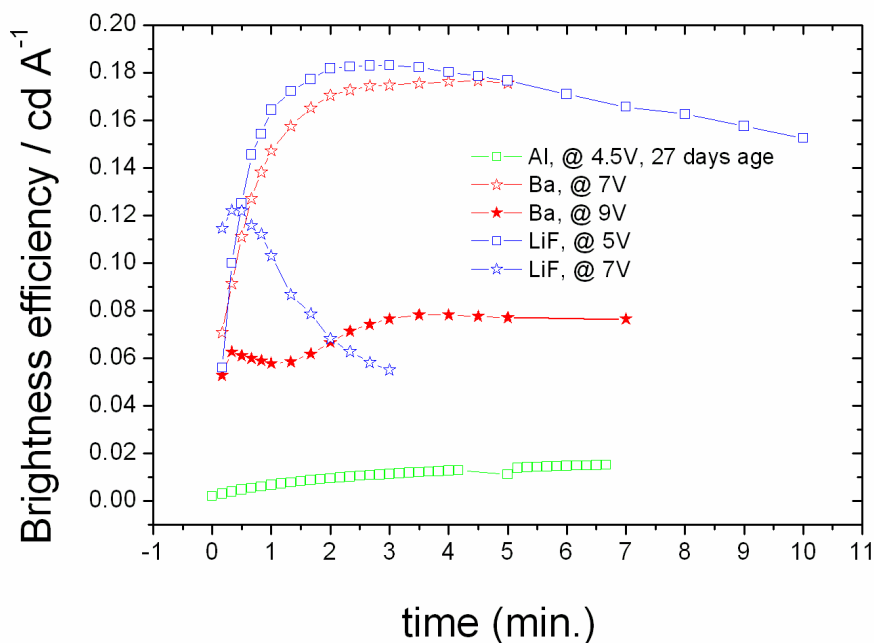


Fig. 5. 9 The Luminescence efficiency against time for O-1F complex with Al (green), Ba (red), and Al/LiF (blue).

The efficiency for these two devices are 0.12 cd/A at 7V and 0.08 cd/A at 9V the maximum, which are lower than found for a smaller charging voltage 5V , which reaches 0.18 cd/A . But it is interesting that for the LiF device which was charged at 7V , the efficiency reaches a maximum at 30 s along with an increase of the current. However from 30 s to 2 min. the current reaches its maximum and remains steady while the efficiency drops by 50% . This suggests the increase of the current is more effective for only one species of carriers, presumably holes in this case. This also happens when

charged at 5V. For the Ba devices, again a very steady equilibrium state for both current and efficiency is observed which suggests Ba might have a better organic/metal interface condition. As for the LiF devices, the hole current is too large and degrades the emitting complex reducing the efficiency. However the LiF device charged at 5V has the best maximum efficiency: 0.19 cd/A.

It is worthy to compare the curves of LiF and Ba devices charged at 7V here to see the difference of these two injection-improve materials. One can see that although the former curve has a larger increase in current and brightness within 2 minutes of charging; the efficiency does not have a corresponding rise. The brightness and efficiency of LiF device decay rapidly in the first few minutes. This means the increase of current in the LiF device is mainly contributed by holes whereas Ba devices have better electron injecting property.

Finally when the Ba device was charged at 9V, although it only increases the current from 30 to 40 mA/cm² in the first two minutes, the brightness increases by a factor of 3. So the balance of electron and hole was improved. However the holes seem still dominate the current.

LiF/Al vs. Alq₃/LiF/Al and BCP/ Alq₃/LiF/Al

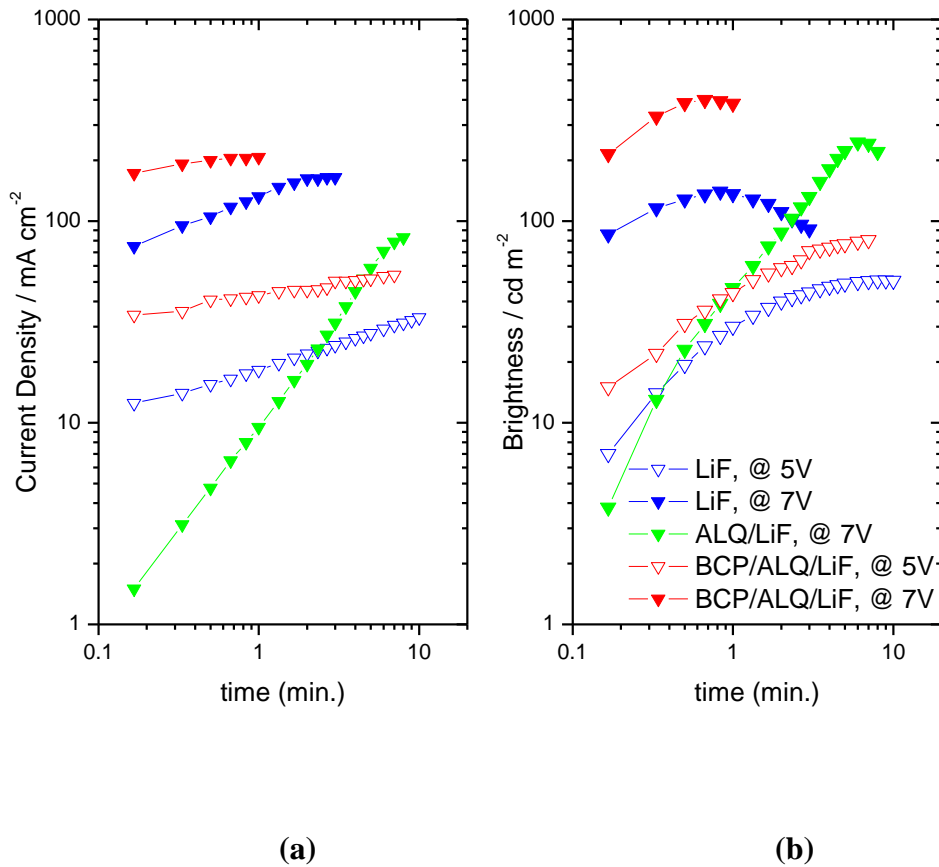


Fig. 5.10 The current density and brightness against time for O-1F complex with Al/LiF (blue), Alq₃/LiF/Al (green) and BCP/ Alq₃/LiF/Al (red)

As usual, Alq₃ and BCP layers were inserted to manipulate the electron injection. First, it is noticed that the Alq₃ devices again begin with the lowest current density. It takes 6 minutes to reach maximum current (80 mA/cm²) and brightness (246 cd/m²) at only 7V. When using an extra BCP layer, the current is highest at both 5V and 7V, and so is the brightness: 80 cd/m² and 400 cd/m². The current increases by a factor of 52 for Alq₃ device, which leads to a dramatic 64.7 times increase in brightness in 8 minutes! For BCP

devices, the increase of current is not obvious: 34->50 mA/cm², but brightness still increase by a factor of 5.3 at 5V.

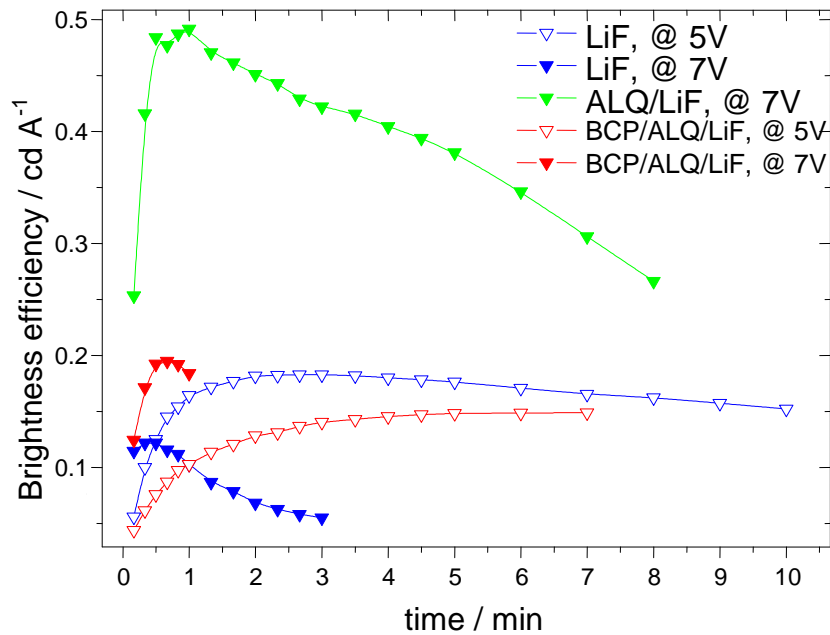


Fig. 5. 11 The Luminescence efficiency against time for O-1F complex with Al/LiF (blue), Alq₃/LiF/Al (green) and BCP/ Alq₃/LiF/Al (red)

As a brief comment here, all the 122(O-1F) devices reach maximum efficiency within 2 minutes. But only the Alq₃ devices can achieve the maximum efficiency of 0.5 cd/A, and the others are all below 0.2 cd/A. However the efficiency of the Alq₃ devices saw decays after passing the maximum value.

124 (O-1F-2C)

Ba/Al vs. LiF/Al, and Alq₃/LiF/Al

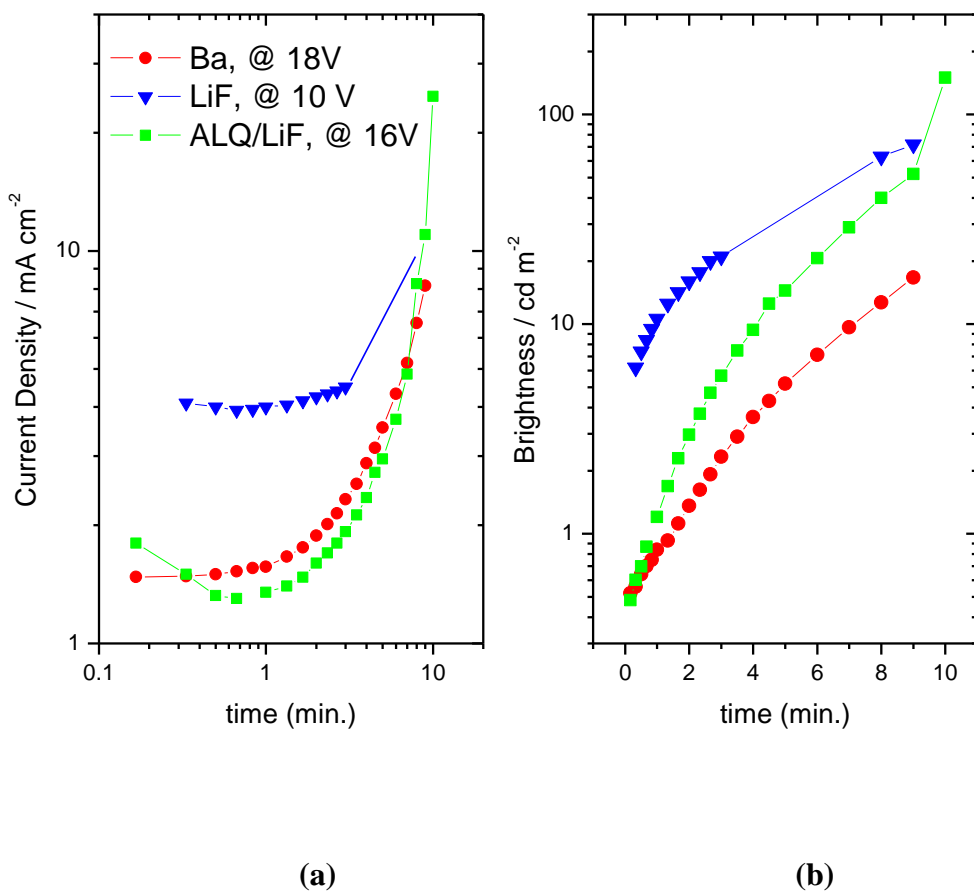


Fig. 5. 12 The current density and brightness against time for O-1F-2C complex with Ba (red), Al/LiF (blue), and Alq₃/LiF/Al (green).

The Ba devices are amazingly bad for the complex 124(O-1F-2C), because the brightness is only about 10cd/m² at 18V. The current is also small considering such a relatively high bias. This might be due to the Ba oxidation during the operation. LiF devices have the highest starting current and brightness, however after 10 minutes, the Alq₃ devices match

up with it in efficiency and brightness. Alq₃ devices have an excellent increase of current and brightness by a factor of 19 and 312 in merely 10 minutes!! However this improvement is not quite so exciting because the maximum brightness and efficiency are similar with LiF device, just it begins from a lower magnitude.

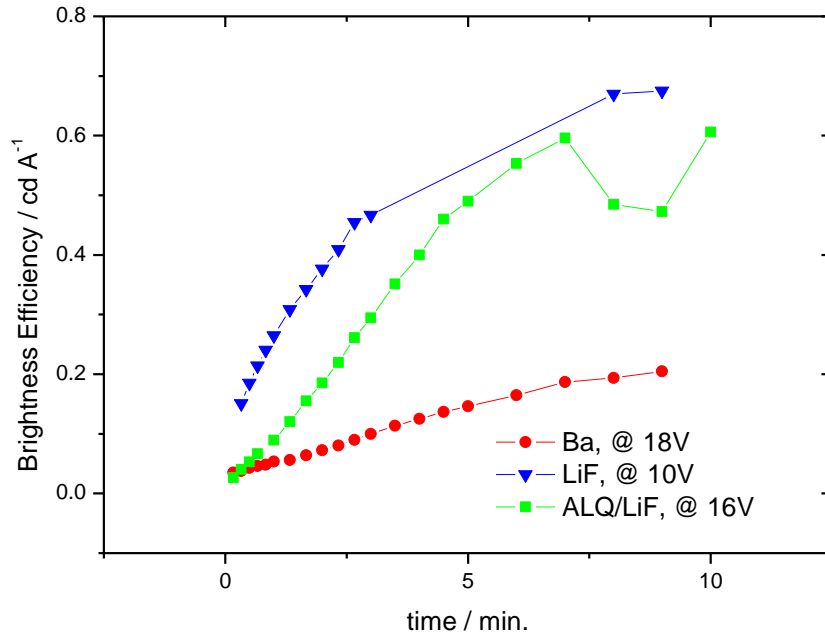


Fig. 5. 13 The Luminescence efficiency against time for O-1F-2C complex with Ba (red), Al/LiF (blue), and Alq₃/LiF/Al (green).

99 (O-2F)

Al vs. Ba/Al and LiF/Al

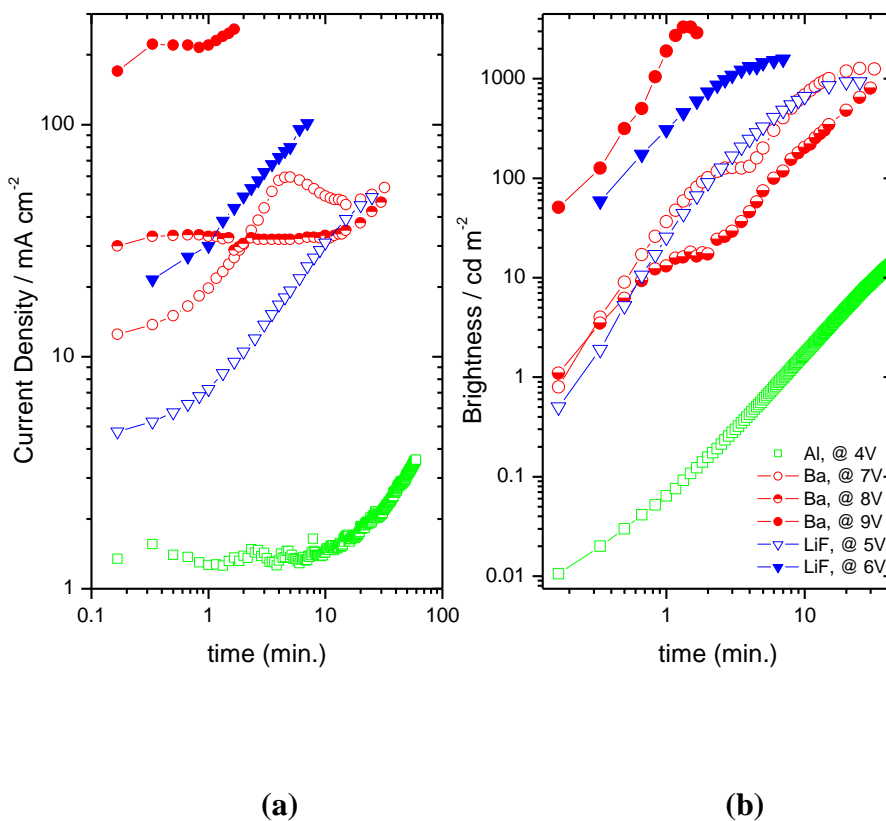


Fig. 5. 14 The current density and brightness against time for O-2F complex with Al (green), Ba (red), and Al/LiF (blue).

The Al only device starts from a current density of 1.3 mA/cm² and increases to 2.3 mA/cm², and brightness from 0.01 cd/m² to 10 cd/m² in 35 minutes when charged at only 4V. This fact shows the potential that this material may have in the Poly LED device. By inserting of LiF layer, the current increases to 4.75mA/m², reaching 48.75 mA/cm², and brightness 0.5 cd/m² which reaches 927 cd/m² in 25 minutes at 5V. At 6V, LiF device easily exceed 1500 cd/m² in 6 minutes. For Ba devices, they require larger current to reach comparable brightness. At 7V, the current increases steeply in the first 5 minutes

and drops after then. This might again due to the Ba oxidation. But after 15 minutes of charging, the brightness reaches 1000 cd/m^2 and keeps its status afterward. At 9V, the current and brightness increase sharply in the first 2 minutes, and the brightness even reach 3300 cd/m^2 at the maximum. However the device could not survive long because of degradation caused by high energy and current.

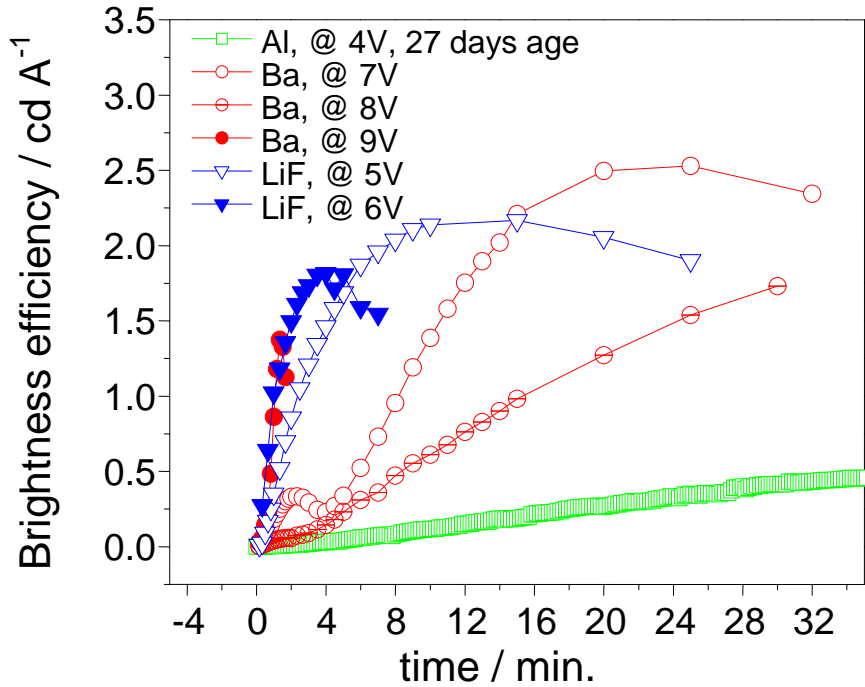


Fig. 5. 15 The Luminescence efficiency against time for O-2F complex with Al (green), Ba (red), and Al/LiF (blue).

Not surprisingly, LiF device again improve efficiency by injecting more electrons: 2 cd/A at 5V compared to 0.45 cd/A at 4V for Al only device. The best performance among the simple structured cathode devices is given by the Ba device charged at 7V, which featured 2.5 cd/A and 1000 cd/m^2 within 20 minutes.

LiF/Al vs. Alq₃/LiF/Al and BCP/ Alq₃/LiF/Al

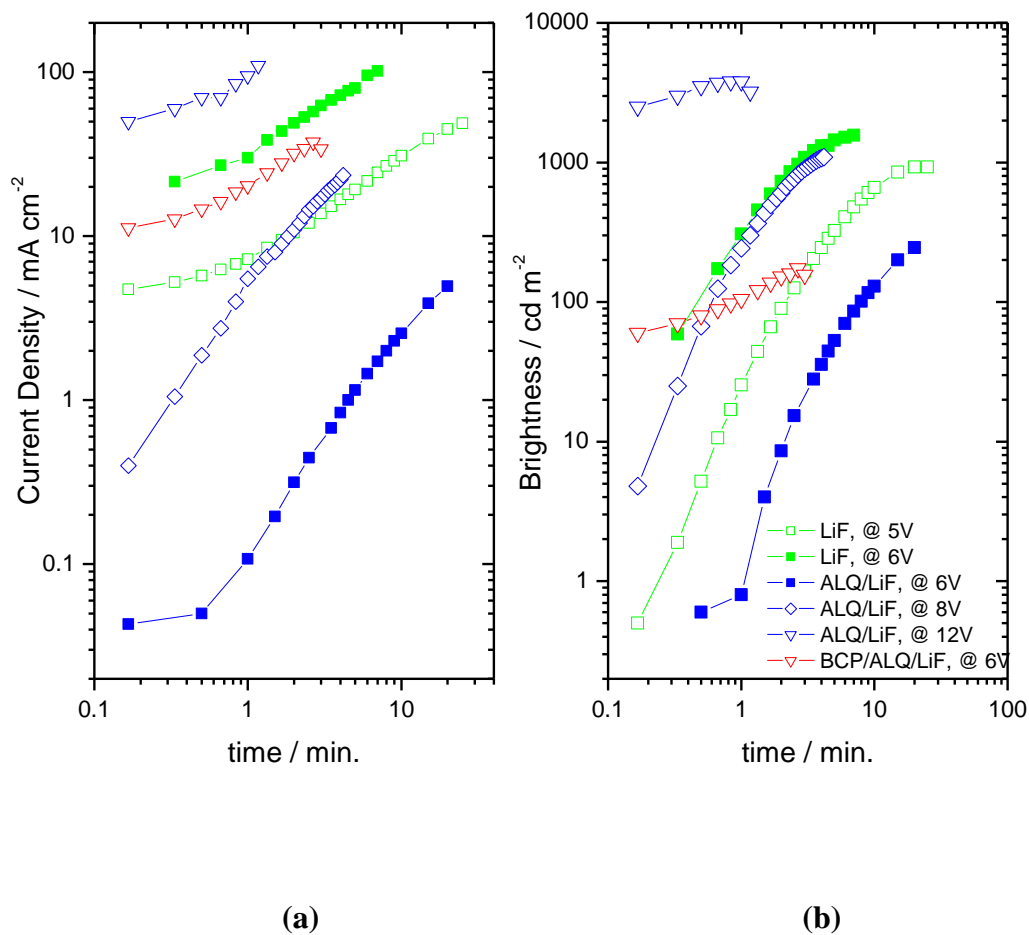


Fig. 5. 16 The current density and brightness against time for O-2F complex with LiF/Al (green), Alq₃/LiF/Al (blue) and BCP/ Alq₃/LiF/Al (red)

The Alq₃ and BCP layers were inserted to block the excess hole current. As observed from the previous tested iridium complexes, for the same charged bias of 6V, Alq₃ device have 2 orders of magnitude lower current density and 1 order of magnitude lower brightness than the LiF counterpart device. Secondly the time required to reach maximum brightness for Alq₃ device is also longer than LiF device. Thirdly at 8V bias, both the brightness and brightness saturation time of Alq₃ device are almost identical with LiF

device at 6V; however the current for the former is slightly smaller which suggests a better efficiency. This proves that the brightness increasing in a LEC device is affected by the bias across the emitting layer, which would be reduced by any additional layers. This also explains why the brightness of BCP device at 6V is much smaller than LiF device at 5V.

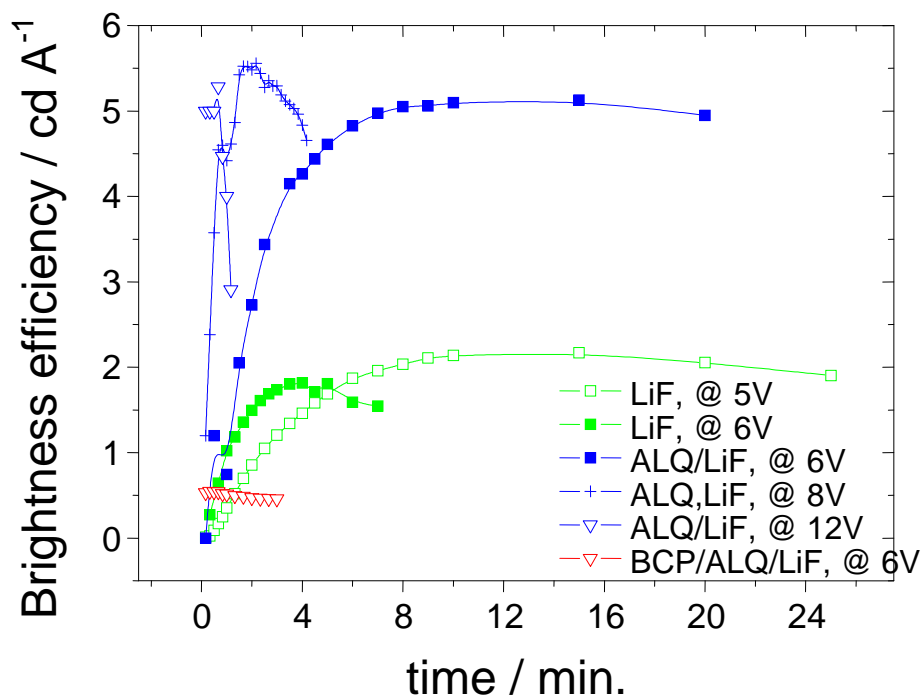


Fig. 5. 17 The luminescence efficiency against time for O-2F complex with LiF/Al (green), Alq₃/LiF/Al (blue) and BCP/ Alq₃/LiF/Al (red)

Although Alq₃ devices have different brightness at 6V, 8V, and 12V, their efficiency are all between 5 cd/A and 6 cd/A, which are about 2.5 times more efficient than LiF only devices. However the efficiency drops quickly at higher driving bias despite the current density is still under 100mA/cm². At this range of current density, the LiF only device

still works well. Therefore the efficiency reduction might come from the 99(O-2F)/Alq₃ interface but not from the degradation of the complex itself.

5.3.3 Summary

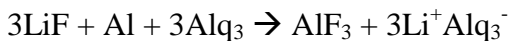
In summary, from the above 2 sections, since the anode was kept the same: ITO/ PEDOT, the different characteristic of current and EL performance of the devices out of the same emitting iridium complex material therefore can be considered coming from the variation of the charge carriers balance inside the devices coming from the cathode.

The two-step increasing behaviour of the current density is observed for almost all devices. The larger charging bias undoubtedly would shorten the required time to reach the equilibrium state of the device. The mechanism of current injection improvement for LiF cathode and Ba cathode is similar according to the similar current behaviour against time. But with the same charging bias, LiF devices have higher current density and brightness as Fig. 5.8 and 5.14. However the barium buffered device provided the best stability during operation among all the three simple structured devices.

To insert an additional Alq₃ layer would be a good idea because it can increase the efficiency by providing better electron injecting and hole blocking, and there seems to be little issue at the Alq₃/complex interface according to their steady performance.

It is worth noting here about why the initial current density of the Alq₃ devices is always lower than the LiF buffered devices. First, they both have the same anode, ITO, therefore the only difference is electron injecting ability of the cathode. The benefit of Alq₃/LiF/Al structure has widely been reported and used¹⁴ in OLED devices. The use of LiF buffer

layer in the structure is studied carefully as well. For the LiF device, the electron injects by tunnelling and the Alq₃ device, the electron injects into the Alq₃ layer by the chemical reaction shown below:



The Gibbs free energy of this reaction is nearly zero. Therefore the migration of PF₆⁻ in the emitting layer does not change the injecting barrier from the metal for Alq₃ devices.

The electron transports through the Alq₃ layers and accumulates at the (iridium complex)/Alq₃ interface. But eventually, this barrier will be modified by interface ions as well and therefore pulls the electron into the emitting layer. This process takes more time than directly modifying the barrier at organic/metal interface.

An extra BCP layer between iridium complex layer and Alq₃ layer does not improve the device performance effectively by blocking the holes and there seems to be an interface issue (defects) between iridium complex layer and BCP layer. The crossing bias through the device plays an important role in determining the time required to reach the equilibrium state. It is reasonable to assume that the higher bias the shorter saturation time it is required. Therefore the additional layers such as Alq₃ and BCP will reduce the bias across the iridium complex layer and extend the charging time, although it does help the electron transporting. Therefore to improve the intrinsic electron mobility in the emitting layer by modifying the complex structure itself or mixing the electron transporting species with the iridium complex layer and keep the electrode as simple and stable as possible. This should be the key to improve the LECs devices in the future.

5.3.4 Comparison of different ligands

Methodology definition

This section is focused on the effect of different ligands attached to the iridium in the complexes main bone. Only the simple structured cathode devices, i.e. Al, LiF, and Ba devices, are used to compare in order to keep it as simple and clear as possible. And from the curves of current density, brightness and brightness efficiency against time, the devices are studied through the turn-on time (TOT), time to reach maximum value (TTM) and the main slope against time (MS). In table 3.1 to table 3.3, the parameters in the boxes filled with red colour indicate that the data is obtained from the figures of current vs. time; for the green boxes, the data is from figures of brightness vs. time; for the blue boxes, it is from figures of efficiency vs. time.

The Effect of Fluorene (Family 2)

	Max Current (mA/cm ²)			TOT (min.)	Max Brightness (cd/m ²)	TTM (min.)	MS	Max Efficiency (cd/A)	TTM (min.)	MS
Al	1F	5V	20	1	3	10	0.5	0.02	10	0.46
	2F	4.5V	4	10	10	40+	1.5	0.5	40	1.34
Al/LiF	1F	5V	30	N/A	35	1	0.5	0.18	2	0.6
	2F	5V	45	1	800	10	2	2.2	10	1.94
Ba	1F	7V	40	N/A	70	1	0.84	0.17	2	0.4
	2F	7V	55	0.8	1000	10	2.2	2.5	20	1.71

Table 5. 2 The comparison between the iridium complex with 1 fluorene and 2 fluorene ligand by major device performance against time.

The Characteristic of 1F and 2F iridium charged complex is summarized in [Table3.1](#). First to be noticed is that 2F iridium complex has better solubility. For each of the cathodes, 2F devices require a longer charging time. However higher brightness, better efficiency, and larger current are generally observed from the 2F devices. Brightness of the devices always saturates while efficiency reaches a maximum then decrease for LiF devices and one of the Ba devices. The fact that the 2F devices need a longer charging time is not surprising since they have bulkier ligands that might impede the migration of PF_6^- ions. The additional fluorene unit not only make the structure symmetric, but dramatically increases both brightness, by a factor of 23, and efficiency, by a factor of 15 at maximum. The main slope is calculated from the log-log plot therefore represents some sort of the power law to the charging time. An additional fluorene has somehow changed the power law of the EL properties against charging time by affecting the migration access of PF_6^- . Generally speaking, the 2F devices perform better than the 1F devices. Although the current has a turn on behaviour, however this does not lead to the increase of efficiency. For example, the 2F Al device has the turn on current after 11 minutes but this is also when the efficiency begins to saturate. This suggests the increase of current after the turn-on point might be contributed from single species of charge carrier only.

The Effect of Carbazole

	Max Current (mA/cm ²)			TOT (min.)	Max Brightness (cd/m ²)	TTM (min.)	MS	Max Efficiency (cd/A)	TTM (min.)	MS
	Al	1F	5V	10	N/A	5	N/A	1.78	0.05	30
2C		7V	4	2	300	4	1.05	7	105	0.48
LiF	1F	7V	5	1	10	0.8	0.87	0.25	7	0.38
	2C	14V	2	2	5	0.6	0.9	0.3	10	0.65
Ba	1F	6V	1	1	2	1	0.76	0.17	N/A	0.3
	2C	12V	20	2	70	2	1.17	0.45	10	0.5

Table 5.3 The comparison between the family 1 iridium complex with 1 carbazole and 2 carbazole ligands by major device performance against time

	Max Current (mA/cm ²)			TOT (min.)	Max Brightness (cd/m ²)	TTM (min.)	MS	Max Efficiency (cd/A)	TTM (min.)	MS
	LiF	1F	5V	30	N/A	35	1	0.5	0.18	2
2C		10V	5	1.5	80	2	1.1	0.7	8	0.51
Ba	1F	7V	40	N/A	70	1	0.84	0.17	2	0.4
	2C	18V	200	6	20	2	1.7	0.2	8	0.74

Table 5.4 The comparison between the family 2 iridium complex with 1 carbazole and 2 carbazole ligands by major device performance against time

The effect of carbazole units in the case of both family 1 and family 2 is summarized in [Table 5.3](#) and [Table 5.4](#). The presence of carbazole makes the charging time slightly longer, which is due to the bulkier ligand structure. It also requires a larger voltage to reach a comparable brightness with the non-carbazole devices. This is different from the effect of the additional fluorene which was compared in the previous paragraph. The extra fluorene ligand does not lead to larger required driven voltage. This suggests that either the 2C devices were made poorly or the addition of carbazole ligand would change the LUMO and HOMO level of the complex. If comparing the slope from the log-log plot, carbazole also changes the PF_6^- migration behaviour by increasing the power law against time by a factor of 2. For the 2C Ba device, the current has a turn on behaviour at about 10 minutes. But it is also observed that this ramping of current does not improve the efficiency after the equilibrium status was reached similar to what happened to the 2F devices.

In conclusion, the carbazole units do not help the charge carrier balance in the device as one had hoped. Instead they might modify the energy level of the iridium complexes and change the energy scheme of the whole device structure. The 2F devices perform best. Although the additional fluorene ligands impede the migration of cations, they seem to provide the better stability in structure that increases the triplet lifetime and the quantum yield of the LEC devices. (The lifetime study is in next section.)

5.3.5 Phosphorescence lifetime study

To understand more about the effect of these different ligands, their photoluminescence decay in the solid state were also measured as shown in Fig. 5.18. Because the pendant side groups will increase the intermolecular separation of the complex, it might reduce the energy transfer between neighboring emitters through Förster energy transfer, which is expected to be dominant over electron exchange Dexter type transfer given the non-negligible triplet absorption of the heavy metal complexes. None of the materials investigated exhibits a single exponential lifetime. Instead the decay rate proceeds faster initially when the excitation density quenched by annihilation processes, and slows down at longer times, thus the decay is dispersive. The half lives fall in the range of 150 to 250 ns, compared to $\sim 1\mu\text{s}$ for typical iridium complexes.

The complex P-1F and O-1F are linked with just a single fluorene unit therefore they pack relatively closely and suffer most from migration activated quenching, which translates into the fastest observed decays within these group of materials. The complex that is most heavily substituted, complex O-2F-4C consistently shows the longest decay time and P-1F-2C, O-1F-2C, and O-2F with their medium-size side chains also exhibit intermediate decay times compared to the above extremes. At long times the decay of complex O-2F-4C becomes non-dispersive as it asymptotically approaches an exponential lifetime of $\sim 2\mu\text{s}$. If assuming this to be the unquenched radiative lifetime of all complexes then the emission quantum yields in solid state relative to the radiative yield would be 21, 32, 19, 35, 30, and 43% for complex P-1F, P-1F-2C, O-1F, O-1F-2C, O-2F, and O-2F-4C respectively by assuming that $\phi = \frac{\tau_{fl}}{2\mu\text{s}}$, where ϕ indicates the

radiative yield and τ_{fl} is the lifetime for each complex. These values on the one hand

show an increase in the PL yield of more than 100 % by increasing the length and number of the linear side chains, but on the other hand imply that even for the best complex O-2F-4C; 60 % of the emission is lost by concentration quenching. Therefore, there is still a significant potential to further increase the emission yield of these cationic iridium complexes.

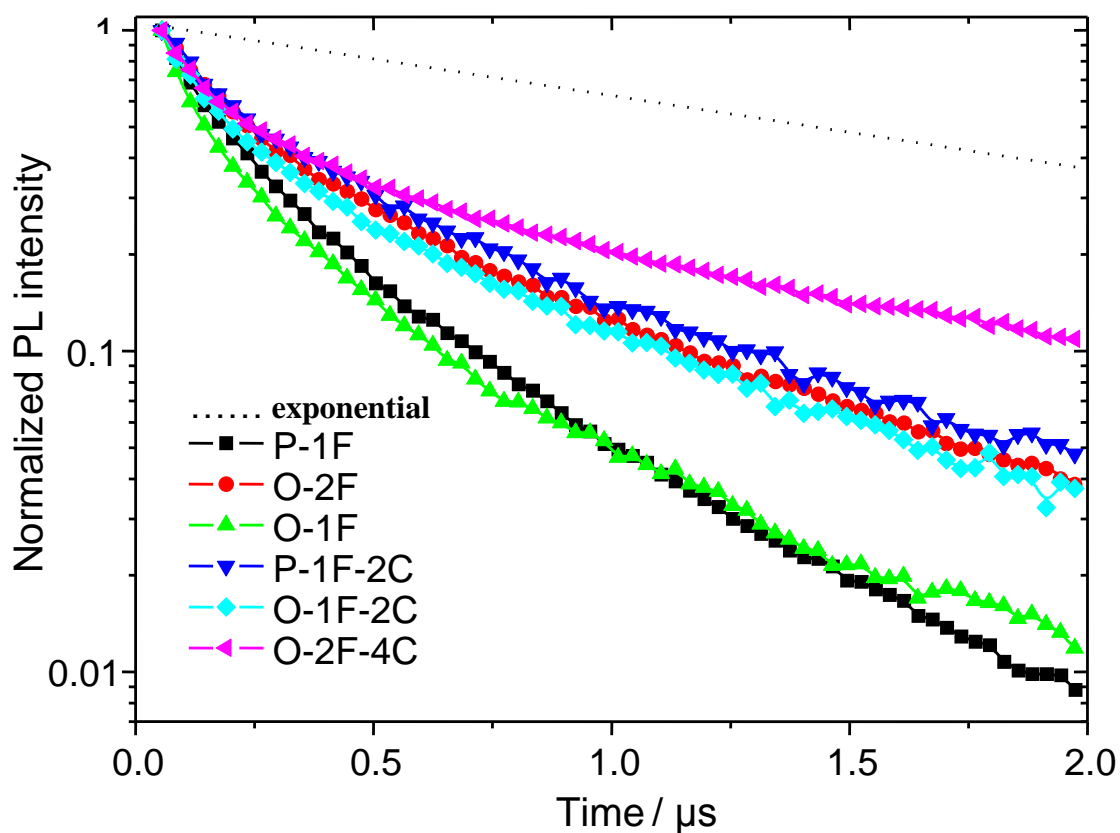


Fig. 5. 18 The PL density decay against time of all the iridium complexes in this thesis. The additions of fluorene and carbazole units lengthen the lifetime of excitation. The dashed line indicates an exponential decay with 2 μ s lifetime.

5.3.6 Highlight of the LEC devices

The key for good LEC device, however, is the quality of the iridium complex solution from which the devices were spin-coated. Because these are all newly synthesized materials, and the amount of them supplied by the Chemistry Department is limited. Therefore there was little chance to properly try out the best solute conditions by using acetonitrile, toluene, or others as the solvents. When the complex dissolved poorly, the devices have the appearance of the scales of a fish in the emitting area. But if it dissolved well, one immediately can have an efficient and homogeneously emitted device with only aluminium as the cathode. But unfortunately, only 2 such good devices were fabricated with high quality in this study. They are made of O-2F-4C and P-1F-2C complexes with Al only cathode, and featured 260 cd/m² and 7 cd/A when charged at 7V which improves to 1000 cd/m² and 7.8 cd/A when charged at 9V (see [Fig.5.19.](#)) They still have quite good quality after operating for 1 week in air (see [Fig.5.20.](#)) although the defects were observed. This is because of oxidation of cathode or humidity within the PEDOT or degradation of the complex. They may be reduced if the devices were hermetically sealed.

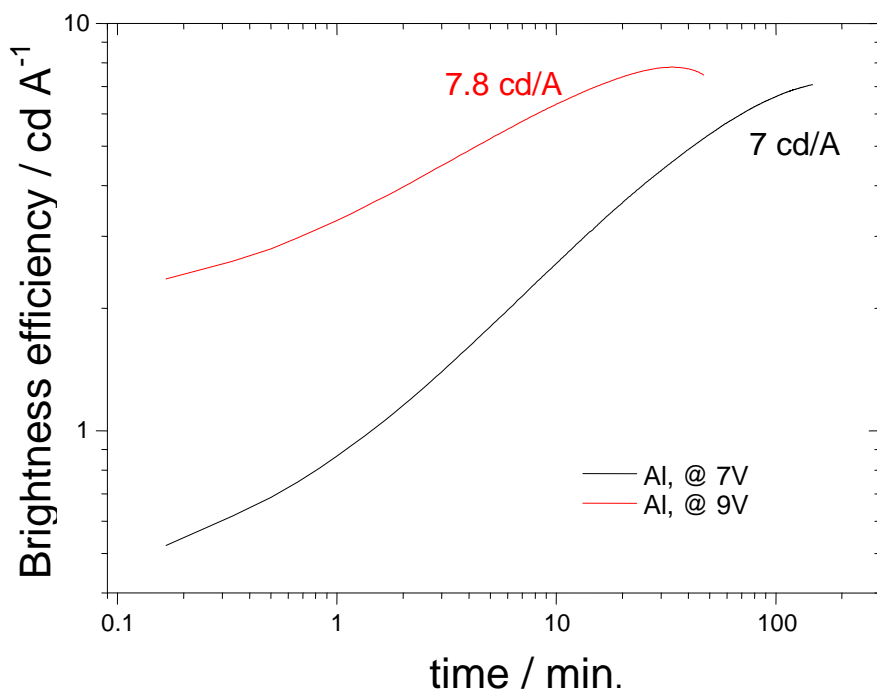


Fig. 5. 19 The luminescence efficiency against time for P-1F-2C complex with Al only cathode at 7V (black) and 9V (red)

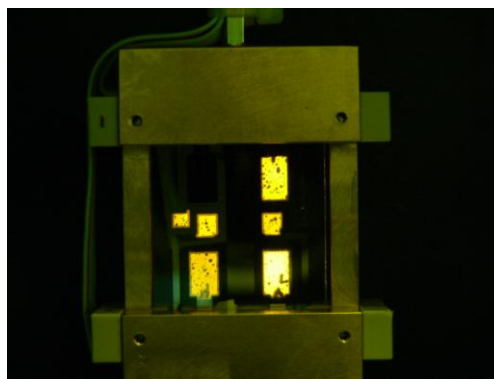


Fig. 5. 20 The picture of the O-2F-4C complex device with Al only cathode. The device has a circle dark point after a few hours of driving which is common for Poly LEDs due to oxidation.

5.4 Conclusion

The current density, brightness, and efficiency for different kinds of cathode and emitting iridium complex were measured. The effect of different ligand structure on phosphorescence lifetime was also studied. It was found that these ligands, although nonconjugated to the main emitting iridium complex, do play an important role in adjusting the charging time, the charging rate, and even the maximum brightness and efficiency of the devices. Generally the more massive the ligand is, the longer the phosphorescence lifetime it has. But the charging time required to reach maximum brightness efficiency is also longer. Take the aluminium devices for example, the charging time required is extended by a factor of 4 by attaching a fluorene ligand and a factor of 3 by attaching the carbazole units. Despite of this, the additional fluorene ligand improves the device efficiency by a factor of 10; on the contrary the additional carbazole only improves by a factor of 2 to 5. This might because of the hole transporting characteristics of the carbazole units increasing the imbalance of charge carriers in the device or modifying the LUMO and HOMO levels of the original iridium complex. The cathode evaluation of aluminium, barium and lithium fluoride as buffer layers showed that the choice of cathode can also be important. Barium buffered devices generally show better stability during operation. Multi functional layers were also introduced into the LEC structure. Although this has increased the required charging voltage by reducing the bias dropped across the iridium complex layer, the Alq₃ devices do show better EL performance by improving the electron injection into the device. However these devices are not as stable as the simple structured cathode devices.

Finally the log-log plots of EL properties against charging time show the current density and the brightness both have some sort of power law against charging time before reaching saturation. At higher driving voltages, the current and the brightness sometimes show turn-on behavior (change of gradient in the log-log plot). The reason for this is still unclear. But the fact that the carbazole devices show a smaller slope than the fluorene devices in the plot of Current/Brightness against Charging time suggests the performance of LECs can be improved by choosing different species of ligands. In this study the fluorene ligand does better than the carbazole units.

Future work to improve the charge carrier balance should focus on the attachment of a smaller sized, electron-transporting, and soluble ligand. A method to decrease the charging time after an initial turn-on by introducing a media in the emitting layer to lock the anions at the metal/complex interface would also greatly improve device performance. However, with relatively simpler device structure and fabrication process than the OLED devices, and the better efficiency and stability than Poly-LED devices, this work has given us a hint about the bright future of LEC devices.

References:

1. M. A. Baldo, D. F. O'Brien, Y. You, A. Shoustikov, S. Sibley, M. E. Thompson and S. R. Forrest, *Nature* **395** (6698), 151-154 (1998).
2. C. Rothe, S. King and A. P. Monkman, *Physical Review B* **73** (24) (2006).
3. A. van Dijken, J. Bastiaansen, N. M. M. Kiggen, B. M. W. Langeveld, C. Rothe, A. Monkman, I. Bach, P. Stossel and K. Brunner, *Journal of the American Chemical Society* **126** (24), 7718-7727 (2004).
4. J. K. Lee, D. S. Yoo, E. S. Handy and M. F. Rubner, *Applied Physics Letters* **69** (12), 1686-1688 (1996).
5. J. Slinker, D. Bernards, P. L. Houston, H. D. Abruna, S. Bernhard and G. G. Malliaras, *Chemical Communications* (19), 2392-2399 (2003).
6. H. Rudmann, S. Shimada and M. F. Rubner, *Journal of the American Chemical Society* **124** (17), 4918-4921 (2002).
7. M. K. Nazeeruddin, R. T. Wegh, Z. Zhou, C. Klein, Q. Wang, F. De Angelis, S. Fantacci and M. Gratzel, *Inorganic Chemistry* **45** (23), 9245-9250 (2006).
8. G. F. He, M. Pfeiffer, K. Leo, M. Hofmann, J. Birnstock, R. Pudzich and J. Salbeck, *Applied Physics Letters* **85** (17), 3911-3913 (2004).
9. S. Sinha, C. Rothe, R. Guntner, U. Scherf and A. P. Monkman, *Physical Review Letters* **90** (12) (2003).
10. J. D. Slinker, C. Y. Koh, G. G. Malliaras, M. S. Lowry and S. Bernhard, *Applied Physics Letters* **86** (17) (2005).
11. H. Kanai, S. Ichinosawa and Y. Sato, *Synthetic Metals* **91** (1-3), 195-196 (1997).
12. D. M. Pai, J. F. Yanus and M. Stolka, *Journal of Physical Chemistry* **88** (20), 4714-4717 (1984).
13. A. B. Tamayo, S. Garon, T. Sajoto, P. I. Djurovich, I. M. Tsyba, R. Bau and M. E. Thompson, *Inorganic Chemistry* **44** (24), 8723-8732 (2005).
14. M. G. Mason, C. W. Tang, L. S. Hung, P. Raychaudhuri, J. Madathil, D. J. Giesen, L. Yan, Q. T. Le, Y. Gao, S. T. Lee, L. S. Liao, L. F. Cheng, W. R. Salaneck, D. A. dos Santos and J. L. Bredas, *Journal of Applied Physics* **89** (5), 2756-2765 (2001).